DOI: 10.1002/adma.200600277

Optical Bandgaps of π-Conjugated Organic Materials at the Polymer Limit: Experiment and Theory**

By *Johannes Gierschner*,* *Jérôme Cornil*, and *Hans-Joachim Egelhaaf*

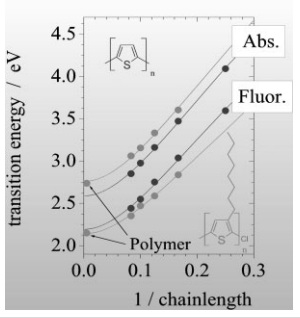

In this Review, the extreme care that must be taken when predicting the optical properties of conjugated polymers via the oligomer approach, and when comparing theoretical and experimental data, is illustrated. In the first part, conceptual strategies for the correct determination of optical transitions from experimental spectra and relevant extrapolation procedures at the polymer limit are introduced. The impact of conformational, substitution, solvent, and solid-state effects on the optical properties is discussed in light of experimental data reported for molecular backbones based on phenylene, phenylenevinylene, and thiophene repeat units. A comparison is then made between experimental results and those provided by standard quantum-chemical methods, to assess their reliability.

1. Introduction

The rational design of all-plastic optoelectronic devices that are based on π-conjugated polymeric materials,[1] such as poly(*p*-phenylene vinylene) (PPV) and polythiophene (PT) (see Fig. 1), is a challenging issue that involves experimental

[*] Dr. J. Gierschner, Dr. J. Cornil
Laboratory for Chemistry of Novel Materials
Center for Research in Molecular Electronics and Photonics
University of Mons-Hainaut
Place du Parc 20, 7000 Mons (Belgium)
E-mail: johannes@averell.umh.ac.be
Dr. J. Gierschner, Dr. H.-J. Egelhaaf
Institute for Physical and Theoretical Chemistry
University of Tübingen
Auf der Morgenstelle 8, 72076 Tübingen (Germany)
Dr. H.-J. Egelhaaf
Christian-Doppler Lab for Surface-Optical Materials
Konarka Austria R&D GmbH
Altenberger Str. 69, 4040 Linz (Austria)

[**] The work in Mons was partly supported by the Belgian Federal Government "Interuniversity Attraction Pole in Supramolecular Chemistry and Catalysis, PAI 5/3", the Technological Attraction Pole SOLTEX, and the Belgian National Fund for Scientific Research (FNRS/FRFC). J. C. is an FNRS Research Associate.

Oligophenylenes *n*P $N = 2n$

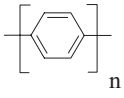

Oligophenylenevinylenes *n*PV $N = 3n + 2$

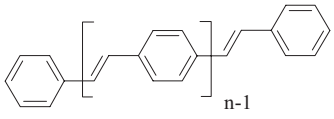

Oligothiophenes *n*T $N = 2n$

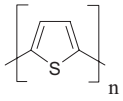

Diphenyloligoenes DP*n* $N = n + 4$

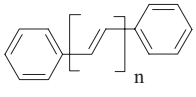

Figure 1. Molecular structures of linear π-conjugated oligomers. *N* is the number of double bonds along the shortest path connecting the terminal carbon atoms of the molecular backbone.

and theoretical chemistry and physics. The performance of the materials is largely inherent to the intrinsic electronic, optical, and photophysical properties of the constituting chains, but is also driven by intermolecular effects, which are governed by the nature of the chain packing and the morphology of the samples.[2]

In order to support, or even guide, the synthesis of novel materials with enhanced properties, quantum-chemical methods are increasingly applied, in particular for the prediction of the optical properties of π-conjugated polymers. The optical bandgap is a key parameter that controls, for instance, the nature of the electroluminescence signal in light-emitting diodes and the efficiency of light absorption in solar cells. A vast amount of data has been accumulated over the years for a variety of materials (differing by their molecular backbone and/or substitution pattern) and with different theoretical methodologies. The vast majority of these approaches follow the so-called oligomer approach, in which the properties of oligomers of increasing chain length are first calculated, and then extrapolated to ideal infinite polymers.[3–5] However, the theoretical and experimental results obtained for a given conjugated backbone generally differ significantly, so that assessing the reliability of a given methodology for the prediction of the polymer properties is a difficult task; as a result, "rules of thumb" have been suggested to yield reliable estimates of optical properties.

Most of the discrepancies observed when comparing experimental and calculated data originate from i) the lack of a full consideration of the parameters that determine the optical properties of π-conjugated polymers, such as conformational

Johannes Gierschner, born in Berlin (Germany) in 1966, received his Ph.D. at the University of Tübingen in 2000. Working as a researcher and academic teacher at the Institute of Physical and Theoretical Chemistry, University of Tübingen, until 2004, he went to the University of Mons-Hainaut and to the Georgia Institute of Technology with Jean-Luc Brédas. His main interests lie in the experimental and theoretical understanding of optical and photophysical properties of organic conjugated materials in solution and supramolecular assemblies. He is the co-author of 27 articles in the field.

Jérôme Cornil was born in Charleroi (Belgium) in 1970. He received his Ph.D. in Chemistry from the University of Mons-Hainaut in 1996, and completed postdoctoral stays at UCSB (with Alan Heeger) and MIT (with Bob Silbey). He is Research Associate of the Belgian National Fund for Scientific Research (FNRS) in Mons and holds a Visiting Principal Research Scientist position at the Georgia Institute of Technology since 2005. His main research interests deal with the theoretical characterization of the electronic and optical properties of organic conjugated materials used in optoelectronic devices. He is the co-author of 150 publications.

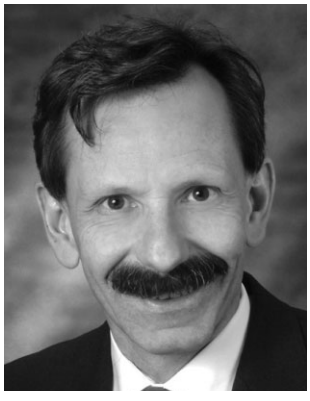

Hans-Joachim Egelhaaf was born in Esslingen (Germany) in 1958. He received his Ph.D. in Physical Chemistry from the University of Tübingen in 1996 for fluorescence spectroscopic investigations on oligothiophene solutions and films. After finishing his habilitation thesis in 2005, on chemical reactivity in polymeric microreactors, he joined the ultrafast optical spectroscopy group of Guglielmo Lanzani at the Politecnico di Milano. Presently he is a Christian-Doppler research fellow in Linz, Austria, and works with Konarka Technologies on organic solar cells.. He is the co-author of 65 publications.

effects, substitution effects, and both solvent and solid-state effects; ii) the general confusion between vertical and adiabatic transition energies; iii) inappropriate extrapolation procedures; and iv) the use of inadequate theoretical frameworks to describe optical transitions in these systems. In this Review, we will clarify the terminology of optical transitions, shortly consider the various empirical, semiempirical, and theoretical extrapolation procedures that have been developed within the last few decades to obtain the polymer values, and describe the main parameters that control the optical properties (Sec. 2). In Section 3, the amplitude of the corresponding effects are estimated from carefully selected experimental data. In Section 4, we assess the reliability of standard quantum-chemical methods in predicting these effects to suggest strategies for a consistent and more accurate prediction of polymer properties that could be exploited for a rational design of these materials. Because the oligomer approach requires calculating the properties of rather large systems, containing up to 100 atoms, the methods herein are restricted to relatively low-cost computational approaches.

Our discussion deals exclusively with materials where the lowest excited state is symmetry-allowed, which is the case for most π-conjugated organic systems. An important exception is polyacetylene and its corresponding oligomers and derivatives, such as diphenyl-polyenes (see Fig. 1).[6] For these molecules, some of the concepts that are developed in Section 2 are not directly applicable. This paper is willing to provide a conceptual approach rather than an exhaustive description of the diversity of materials, substitution patterns, solvent and temperature evolutions, and solid-state effects. The experimental examples selected in Section 3 are therefore restricted to three kinds of molecular backbones, which differ from each other by i) their polarizability, which results from the introduction of thiophene versus benzene rings in the repeat unit; and ii) their steric hindrance, which depends on the introduction of vinylene units between the rings (see Table 1).

2. Basic Concepts

The "optical bandgap"[14] (E_{gap}) of π-conjugated organic molecules is determined by several parameters, among which the electronic transition energy of the unsubstituted planar backbone (E_{bb}) contributes the most, upon photoexcitation. However, other parameters also have a significant impact, with contributions that can sum up to 1 eV, i.e., about 50 % of the absolute value of E_{gap}. Based on the formulation introduced by Roncali,[15] E_{gap} can be expressed as

$$E_{gap} = E_{bb} + E_{dist} + E_{sub} + E_{solv} + E_{cryst} \quad (1)$$

where E_{dist} is the hypsochromic (blue) energy shift induced by distortion from planarity in the equilibrium geometry, E_{sub} the energy shift induced by the positive/negative inductive/mesomeric effects of chemical substituents (in most cases, a negative number), E_{solv} the bathochromic (red) solvent shift compared to the value in vacuo, and E_{cryst} the bathochromic shift induced by intermolecular interactions in the solid state. In order to estimate these effects properly by theoretical methods, the parameters should not only be understood, but also evaluated from the experimental side.

2.1. Optical Transitions

2.1.1. Experimental Determination of the S_0–S_1 Transition Energy

At the molecular level, E_{gap} corresponds to the adiabatic transition energy (E_{00}), depicted in Figure 2. For molecules in which the absorption spectrum mirrors the emission spectrum, E_{00} is easily determined experimentally as the energy at the intersection of the normalized fluorescence and absorption spectra. This situation is encountered for molecules in which

Table 1. Optical properties (in eV) of unsubstituted polymers as determined by the oligomer approach according to Equation 8: Adiabatic transition energies E_{00}, equilibrium energies ΔE_{eq} for emission (em) and absorption (abs) at room temperature (Eqs. 2 and 3), solvent shifts ΔE_{Solv}, (Eq. 10), and crystal shift ΔE_{Cryst}. Last column: experimental adiabatic transition energy of polymer films (taken as the onset of absorption).

				Oligomer Approach						Polymer film
Polymer	Structure	Maximum *n*	Solvent	$E(F_1)$ [eV]	E_{00} [eV]	ΔE_{eq}(em) [eV]	ΔE_{eq} (abs) [eV]	ΔE_{solv} [eV]	ΔE_{cryst} [eV]	E_{00} [eV]
PP		6 [a]	hexane	3.14	3.17	0.18	0.57	–	–	2.85 [b]
PPV	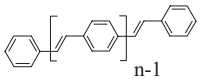	4 (*n*PV) [c]	dioxane	2.62	2.65	0.23	0.28	–0.32	–0.27 [d]	2.38 [e]
		6 (B*n*PV) [f]	CH_2Cl_2	2.58	2.61	0.23	0.28	–	–0.17 [m]	
PT		6 [h]	hexane	2.23	2.26	0.21	0.36	–0.26	–0.32 [i]	2.00 [j]
			CH_2Cl_2	2.19	2.22	0.21				

[a] See Momicchioli et al. [7]. [b] See Kohler [8]. [c] See Gierschner et al. [9]. [d] Taken from comparison with *n*PV nanoparticle spectra. [e] See Friend et al. [1]. [f] 3,5,3′,5′ tetra-(*t*-butyl)-substituted oligo(phenylene vinylene)s (OPVs; B*n*PV) [11]. [g] Taken from comparison with BnPV nanoparticle spectra. [h] See Gierschner et al. [12]. [i] Taken from comparison with *n*T nanoparticle spectra. [j] See Hayashi et al. [13].

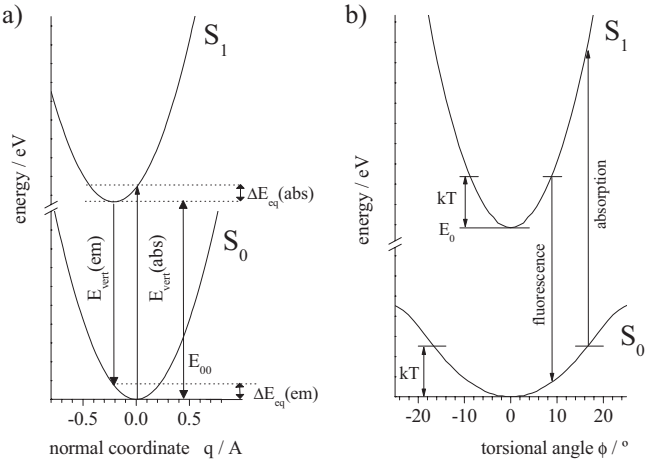

Figure 2. a) Schematic representation of potential energy surfaces for displaced, undistorted harmonic oscillators in the normal coordinate representation coupled to symmetry-allowed, high-energy, in-plane modes. The vertical (E_{vert}(em), E_{vert}(abs)) and adiabatic (E_{00}) electronic transitions are indicated. b) Schematic representation of potential energy surfaces for undisplaced, distorted oscillators coupled to out-of-plane torsional modes [9]. The vertical transitions associated to the emission and absorption processes are indicated.

the geometric changes upon electronic excitation are small, thus implying that the coupling to vibrational modes is similar in the two states. This is fulfilled at any temperature for rigid chromophores, such as oligoacenes and ladder-type oligophenylenes (L*n*Ps).[16] In this case, full mirror symmetry is observed, depicted schematically as A-type in Figure 3. The vertical transition energy (E_{vert}) for absorption (abs) and emission (em) is given by

$$E_{vert}(abs) = E_{00} + \Delta E_{eq}(abs) \quad (2a)$$

and

$$E_{vert}(em) = E_{00} - \Delta E_{eq}(em) \quad (2b)$$

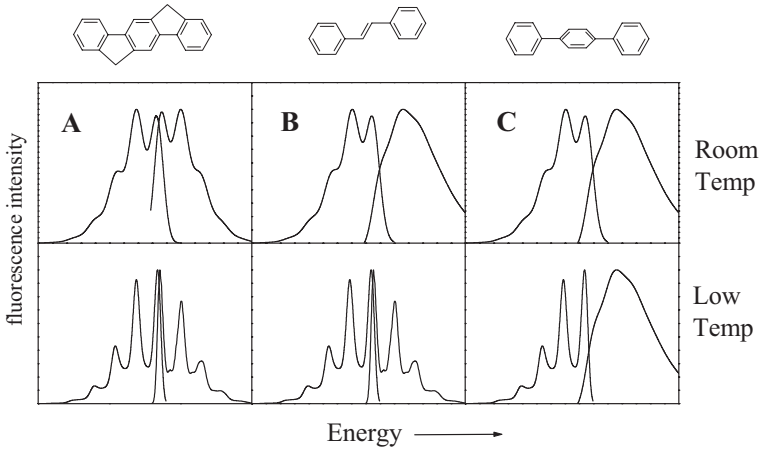

Figure 3. Schematic representation of the emission and absorption spectra of A-, B-, and C-type molecules in solution at room temperature and at low temperature.

where ΔE_{eq} is the equilibration energy (sometimes also referred to as relaxation or reorganization energy, see Fig. 2). Experimentally, E_{vert} for the absorption or emission process can be estimated as

$$E_{vert}(abs) = \frac{\int A(E) \cdot E\, dE}{\int A(E)\, dE} \quad (3a)$$

or

$$E_{vert}(em) = \frac{\int I_F(E) \cdot E\, dE}{\int I_F(E)\, dE} \quad (3b)$$

with $A(E)$ representing the absorbance and $I_F(E)$ the fluorescence intensity at a given energy, respectively. Note that Equation 3a can be applied quantitatively only when no higher-lying electronic transitions are hidden under the low-energy absorption band. If this is the case, the $S_0 \rightarrow S_1$ absorption spectrum can be extracted by a method described earlier:[17] The emission spectrum is mirrored at E_{00} and, where necessary, convoluted by an exponential distribution to account for the different torsional potentials in the S_0 and S_1 states (see below),[9] so that the simulated absorption spectrum $A'(E)$ fits the measured one in the low-energy region. Equation 3a is then applied to $A'(E)$ to extract the actual E_{vert}(abs). When there is perfect mirror symmetry between the absorption and emission spectra, the equilibration energies are equal (see Fig. 2a):

$$\Delta E_{eq}(abs) = \Delta E_{eq}(em) \quad (4)$$

The situation becomes somewhat more complicated for flexible molecules, such as oligo(phenylene vinylenes) (*n*PVs), oligothiophenes (*n*Ts) or oligophenylenes (*n*Ps), the chemical structures of which are shown in Figure 1. In the S_0 state, these molecules exhibit a shallow potential well, associated with torsions around the inter-ring single bonds, so that the excited vibrational states of low-frequency torsional modes are easily accessed by thermal activation. In the S_1 state, these inter-ring bonds are significantly shortened, and much higher frequencies are obtained for the torsional modes compared to S_0 (cf. the different curvatures of S_0 and S_1 in Fig. 2b).[9,18] As a result, the absorption spectra of flexible molecules at elevated temperatures no longer exhibit mirror symmetry with respect to the emission spectra; the absorption spectra are broad and featureless, whereas the emission spectra are still somewhat structured, as shown for the B- and C-types in Figure 3. For B-type molecules (e.g., *n*PVs and long *n*Ts ($n \geq 3$)), the equilibrium geometry is planar in both the S_0 and S_1 states when $T \rightarrow 0$ K, and yields a mirror symmetry. In C-type molecules (e.g., *n*Ps) the equilibrium geometry is nonplanar in the ground state,[19–21] and there is no mirror symmetry between the absorption and emission, regardless of the temperature (Fig. 3c).[22] A different behavior is observed for molecules where the S_1 state is symmetry-forbid-

den in some solvents, such as for biphenyl or diphenyl(polyenes) (DP*n* with $n>1$, see Fig. 1). For these molecules, the $S_0 \rightarrow S_1$ emission is usually masked by the $S_0 \rightarrow S_2$ transition, and exceptionally large apparent Stokes shifts (defined as the energy spacing between the absorption and emission maxima) are observed.[7,23]

If E_{00} cannot be evaluated directly from the spectrum, as is the case in room-temperature spectra of B- and C-type molecules, the position of the lowest vibronic feature of the emission (F_1) is a reasonable first approximation for E_{00}. The "true" adiabatic transition energy E_{00} in a room-temperature spectrum can be also determined by convoluting the highly resolved features observed in the low-temperature emission spectrum with a Gaussian of appropriate bandwidth to account for the temperature effect. An example is given in the inset of Figure 4 for quinquethiophene (5T), showing that E_{00} is located about 30 meV above the highest fluorescence subband F_1. Approximating F_1 as the adiabatic transition energy is appropriate when the broadening of the emission spectrum is not too large. Another reasonable estimate of E_{00} is given by the onset of the absorption spectrum (see Fig. 4a). The latter is frequently used, although it is often hard to determine, especially in samples where light scattering is significant, for example, in spin-coated or vapor-deposited films. The energy at the intersection of the absorption and emission spectra (IS) can also be considered; this slightly overestimates E_{00} by ca. 1 % in Figure 4a.

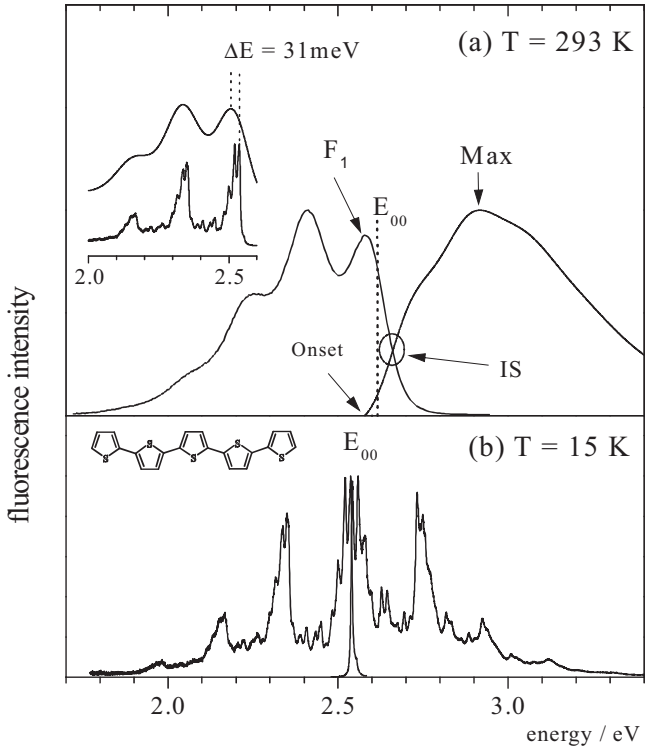

Figure 4. a,b) Fluorescence (left) and absorption spectra (right) of quinquethiophene (5T) in tetradecane at $T=293$ K (a) and $T=15$ K (b) [12]. Inset: low-temperature fluorescence spectrum, convoluted with a Gaussian bandwidth of 1100 cm^{-1}.

For B-type molecules, Equation 4 holds at low temperatures. The equilibration energy for emission (ΔE_{eq}(em)) is slightly affected by an increase in the temperature, because the impact of thermal excitations on torsional modes is small in the S_1 state. For example, the emission spectrum of 5T (Fig. 4) displays a small increase in ΔE_{eq}(em) from 0.21 eV at 15 K to 0.23 eV at 293 K, as deduced from the experimental spectra with Equation 3b. In first approximation, the vertical transition energy of B-type molecules for absorption at 0 K, E_{vert}(abs, $T\rightarrow 0$ K) can be determined from room-temperature emission spectra. To do so, E_{vert}(em) is extracted from the emission spectrum (Eq. 3b), and ΔE_{eq}(em) is calculated by Equation 2b knowing E_{00}. Using Equations 4 and 2a, the vertical transition energy E_{vert}(abs, $T\rightarrow 0$ K) is obtained. This procedure is very helpful, because E_{vert}(abs, $T\rightarrow 0$ K) is directly provided by quantum-chemical calculations. The vertical transition at room temperature (E_{vert}(abs, RT)) is accessible only by using Equation 3a, and deviates from the value at low temperature depending on the width of the distribution of the nonplanar conformers in the S_0 state. The difference ΔE_{th}(abs) is thus a measure of the flatness of the torsional potential in S_0, as described in Equation 5.

$$\Delta E_{th}(\text{abs}) = E_{vert}(\text{abs, RT}) - E_{vert}(\text{abs, } T\rightarrow 0 \text{ K}) \quad (5)$$

For polymeric materials, the absorption spectrum not only reflects the influence of thermal excitation of low-frequency modes, but also a distribution of different actual conjugation lengths.[24] The absorption maximum in polymers therefore represents a mean value of the distribution.[25,26] The adiabatic transition E_{00}, determined from the onset of absorption or from the F_1 band, is representative of the longest actual conjugation length. Similarly, the emission is governed by the intrinsic properties of the longest segments, which are accessed by energy transfer from the shorter segments of the distribution.[24] It is therefore not straightforward to compare the absorption maximum estimated by extrapolation from oligomers and the value directly measured for the corresponding polymer. Adiabatic transition energies are more suitable for comparison, because the experimental value of E_{00} is close to the value expected for an "idealized" infinite polymer chain that is reached by extrapolation within the oligomer approach.

2.1.2. Theoretical Estimates of Transition Energies

Vertical (E_{vert}) and adiabatic (E_{00}) transition energies can be accessed from quantum-chemical approaches at different theoretical levels, and at varying computational costs. Criteria for the assessment of the reliability of standard approaches for the prediction of optical bandgaps are given in Section 4. In some cases, especially for the Hartree–Fock method coupled to a configuration interaction scheme with single excitations (CIS), E_{vert} should not be calculated directly because the slope of the S_1 potential surface is strongly overestimated. In this case, however, it is possible to compute E_{vert} via Equation 2a by explicitly calcu-

lating E_{00}, obtained from the optimized excited-state geometry; and the equilibration energy ΔE_{eq} as[27]

$$\Delta E_{eq} = \sum_k h\nu_k S_k \tag{6}$$

where h is Planck's constant (6.626×10^{34} J s), and ν_k and S_k are the frequencies and Huang–Rhys factors, respectively, of the vibrational modes k coupled to the electronic transition. The Huang–Rhys factors are computed by projecting the normal coordinates of the modes on the geometric changes induced upon electronic excitation by using[27]

$$S_k = \frac{2\pi^2 c}{h} \nu_k (\Delta Q_k)^2 \tag{7}$$

where c is the speed of light (2.997×10^8 m s^{-1}), and ΔQ_k the change in the normal coordinate Q_k between the two electronic states. It is generally assumed here that the vibrational modes are the same in the two states (undistorted harmonic oscillators), and that Duschinsky coupling effects[27] can therefore be neglected. A more general approach takes into account the distortion of the oscillators, providing a general recursion formula for the Franck–Condon factors for distorted, displaced harmonic oscillators.[28] Such models can further include thermal excitations of torsional modes, thus allowing for the simulation of room-temperature absorption spectra of B-type molecules.[9]

2.2. Extrapolation Procedure to the Polymer Limit

To estimate the transition energy of a polymer from the transition energies obtained for the corresponding oligomers, the latter are usually plotted as a function of $1/N$, with N the number of double bonds along the shortest path connecting the terminal carbon atoms of the molecular backbone. A linear relationship is typically observed between the experimental transition energies and $1/N$ for oligomer sizes ranging from 2 to 6 repeat units (n), while the transition energy of the monomer ($n = 1$)deviates from the linear behavior, as illustrated in Figure 5 for oligothiophenes. Because longer oligomers of well-defined chain length ($n > 6$) were not available until the mid 1990s,[29] the linear dependence prevailing for medium-size oligomers stimulated a large number of research groups to extrapolate the oligomer values to the limit of an ideal infinite conjugated polymer chain by linear regression.[30–44] However, the experimental optical bandgaps of oligomers with $n > 6$[45–48] were always significantly larger than the extrapolated values. This became more and more evident with the growing length of soluble oligomers.[11,49] The most prominent example is the synthesis and characterization of well-defined alkyl-substituted oligothiophenes containing up to 96 monomer units by Otsubo and co-workers (see Fig. 6).[46,47] The actual polymer values are always larger than the values obtained by linear extrapolation, provided that the properties of the polymer and those of the corresponding oligomers are measured under the same conditions, i.e., with the same solvent and at the same temperature. In order to quantify this effect,

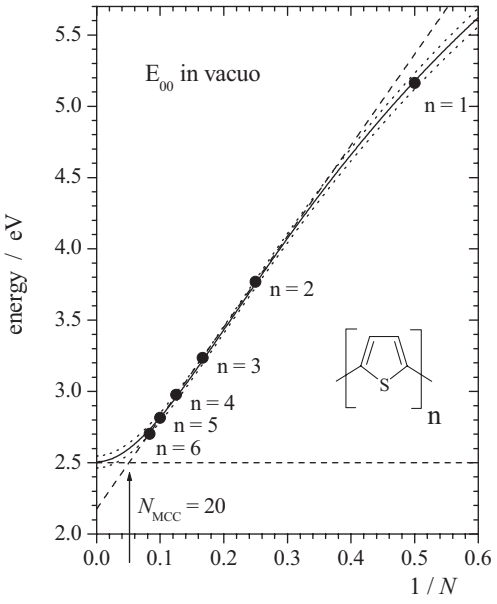

Figure 5. Experimental adiabatic transition energies (E_{00}) of oligothiophenes nT extrapolated to vacuum [12]. For $n > 1$, E_{00} was obtained by the extrapolation method described in Section 2.4, Equation 10. Solid line: Kuhn fit to the oligomer values according to Equation 8. Dotted lines: 95 % confidence bands. Dashed line: linear fit. N_{MCC}: maximum conducive chain length.

Meier et al.[45] intensively discussed the concept of "effective conjugation length" (ECL),[50–53] defined by them as the conjugation length at which the wavelength of the absorption maximum in the series of oligomers is not more than 1 nm

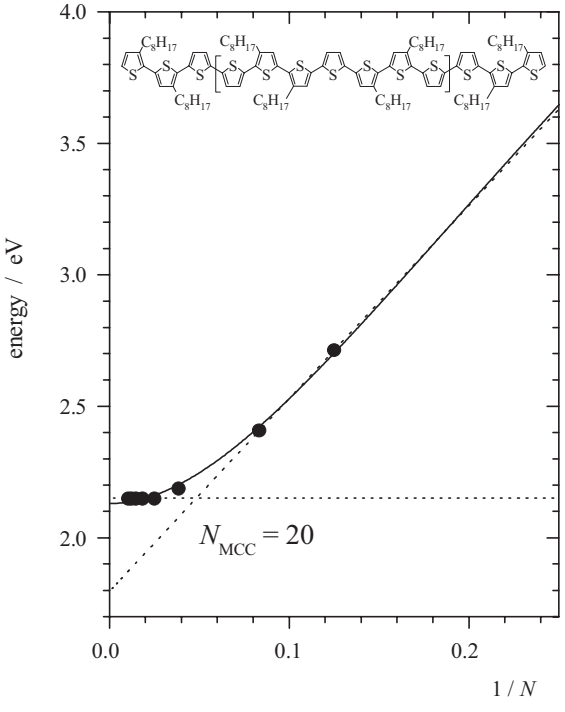

Figure 6. Experimental adiabatic transition energies E_{00} (F_1 positions) of alkyl-substituted oligothiophenes nT up to the 48-mer in dichloromethane [47]. Solid line: Kuhn fit. Dashed line: linear fit.

above the lower limit, which is given by the infinitely long polymer chain. From this definition, the ECL largely differs for the various oligomer series.[45] To obtain a parameter that is less sensitive to the type of oligomers, we introduce the "maximum conducive chain length" (N_{MCC}). The latter is obtained graphically from the plot of transition energies versus $1/N$ as the intersection of the extrapolation of the linear part of the curve (i.e., for short oligomers) with the horizontal line representing the polymer limit (see for example Figs. 5 and 6). When considering the number of double bonds along the shortest path of the molecular backbone, this definition leads to N_{MCC} values typically on the order of 18–22, independent of the nature of the molecular backbone and the substitution pattern. Different effects are likely to contribute to the experimentally observed effective conjugation length,[54] and the roles of these extrinsic and intrinsic effects are described in the following paragraphs.

Extrinsic effects, related in particular to the deviation of the molecular backbones from planarity by thermal activation, the amplitude of which can be estimated by ΔE_{th}, given by Equation 5. Figure 7 collects the values of E_{vert} for the absorption of nT oligomers at $T = 15$ K and at $T = 300$ K, obtained according to the procedure described in Section 2.1. For all nT oligomers, ΔE_{th} is found to be about 0.15 eV, thus indicating that the torsional degrees of freedom of the oligomers do not evolve significantly with chain length, and are therefore not the origin for the ECL. This is confirmed when plotting the optical bandgap of rigid molecules, such as ladder-type oligophenylenes (LnPs),[16] as a function of $1/N$ (Fig. 8). Chemical sp^3 defects, which would also restrict the conjugation length, can be excluded as the source of the ECL.

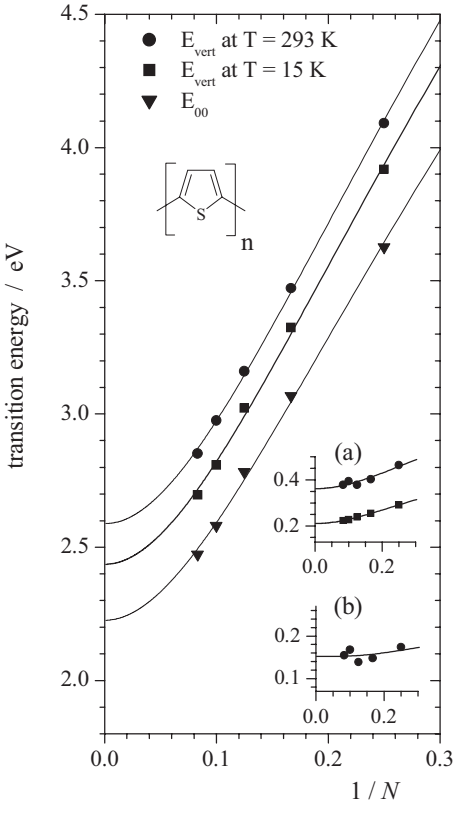

Figure 7. Electronic transitions of oligothiophenes nT ($n = 2$–6) in dichloromethane. ▼: Adiabatic transition energies E_{00} (= F_1 positions +30 meV, as deduced from Fig. 4). ■: Vertical transitions for absorption E_{vert}(abs) at $T \rightarrow 0$ K, according to Equations 2a and 4. ●: Vertical transition energies E_{vert}(abs) at $T = 293$ K according to Equation 3b. Lines are Kuhn fits to the oligomer values according to Equation 8. Insets: a) Equilibration energy for emission, E_{eq}(em) (■) and absorption E_{eq}(abs) (●) according to Equations 2a and 2b, respectively. b) Difference between the vertical transition energies of absorption at $T = 15$ K and $T = 293$ K, ΔE_{th}, according to Equation 5.

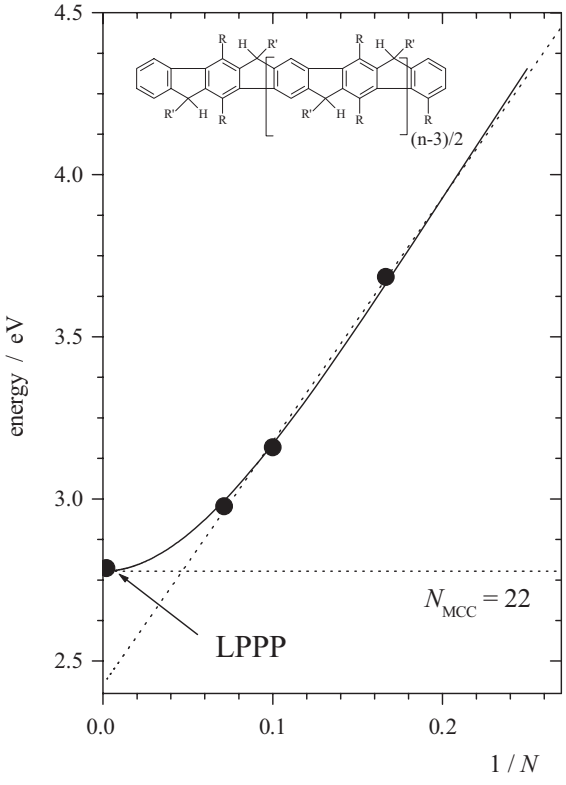

Figure 8. Adiabatic transition energies E_{00} of ladder-type oligophenylenes nLP (estimated at the intersections of the fluorescence and absorption spectra) and of the corresponding polymer in dichloromethane (solid symbols) [16]. Solid lines: Kuhn fit to the oligomer values according to Equation 8. Dotted line: linear fit.

The typical value of the ECL would imply that, on average, every 10th unit of a polymer chain would contain a defect. Such a high defect concentration is not supported by analytical methods applied to the polymers under study.[55]

Intrinsic effects are caused by electron correlation, which leads to bond alternation and the subsequent saturation of the optical transition energies with increasing chain length. Different (semi)empirical extrapolation methods,[56,57] which reproduce this effect, were reviewed by Meier et al.[45] The authors suggested an exponential fit using three empirical parameters, which correctly described the chain length dependence of different oligomeric series with respect to $1/N$.[45] In

a more physical approach based on classical mechanics, W. Kuhn calculated the evolution of the excitation energy with increasing chain length by a model based on the idea of Lewis and Calvin,[58,59] where the formal double bonds of a polyene are regarded as N identical oscillators, each vibrating at an energy $E_0 = h\sqrt{k0/4\pi^2\mu 0}$, where k_0 and μ_0 are the force constant and the reduced mass of the isolated oscillator, respectively. If N adjacent double bonds are coupled with a force constant k', N "eigenmodes" are obtained for the polyene. The lowest energy can be written as[60]

$$E = E_0\sqrt{1 + 2\frac{k'}{k_0}\cos\frac{\pi}{N+1}} \tag{8}$$

with k'/k_0 usually on the order of –0.45. A similar expression is obtained on the basis of a corresponding exciton formalism by Simpson,[61,62] who considered the coupling between the transition dipole moments of the double bonds forming the polyene π-system. In quantum-chemical approaches, such as the "free electron gas model" (H. Kuhn, 1958),[63] the Hückel model,[50,64] and the Peierls–Hubbard model,[54,65] the correct evolution of the transition energies with respect to $1/N$ is obtained by accounting for electron interaction through the introduction of bond alternation parameters in the expression of the resonance or transfer integrals.[66] The correct chain-length dependence is also found with more sophisticated quantum-chemical methods (where electron interaction is explicitly considered), such as the semiempirical Hartree–Fock intermediate neglect of differential overlap (ZINDO) method, as parameterized by Zerner and co-workers,[67,68] PPP (Pariser–Parr–Pople)[69,70] methods, or with ab initio Hartree–Fock approaches coupled to a CIS scheme.[71] Density functional theory (DFT) calculations generally tend to overestimate long-range electron correlation effects,[72] leading to a deviation from the linear behavior only for $n > 10$,[73] as also described in Section 4.2. The localization of the excitation can be visualized by electron–hole two-particle wavefunction plots.[17,54] In such plots, the position of the hole (electron) is varied along the x-axis (y-axis) over all atomic centers, and the probabilities of finding the electron–hole pair at the positions defined by the grid are reported. The amplitude of the off-diagonal ($x \neq y$) elements along a vertical line, which measures the extent of the electron–hole separation, does not further evolve for large values of N, thus indicating that the electron–hole pairs are localized species (i.e., Frenkel excitons). In contrast, the transition dipole moment, which can be estimated from the diagonal elements ($x = y$) of the plots and directly relates to the oscillator strength (f), keeps increasing with chain size (f evolves linearly with N). This implies that the localized species migrate over the whole conjugated path, as can be monitored by single-molecule spectroscopy.[74]

Reliable predictions of the polymer limit by extrapolation methods require the consideration of a larger number of oligomers. An illustrative example is given in Figure 5, where the polymer limit for polythiophene (PT) in solution is determined from nT oligomers, with $n = 1$–6. The prediction of the polymer limit from Equation 8 is in good agreement with the experimental values obtained for soluble polymers (Figs. 8 and 9), as long as the experimental conditions (i.e., substitution pattern, solvent, and temperature) are the same for the oligomers and the polymer, see Section 3.1.

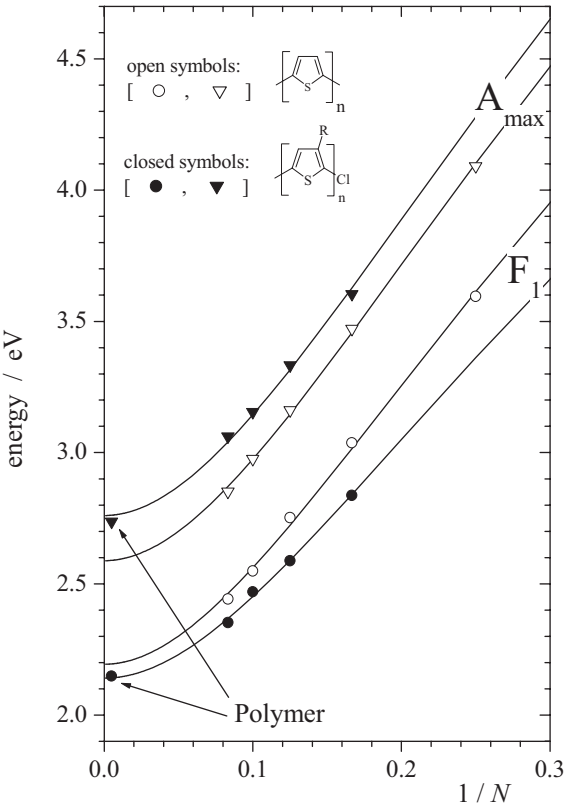

Figure 9. Spectral positions of the absorption maxima (A_{max}; triangles) and of the first fluorescence band (F_1; circles) of unsubstituted oligothiophenes (open symbols) in CH_2Cl_2, regioregular (rr) oligo(3-octylthiophenes) (closed symbols), and rr-poly(3-octylthiophene) in $CHCl_3$ [33]. Lines are Kuhn fits to the oligomer values according to Equation 8.

We also stress that it is necessary to optimize the molecular geometries at the quantum-chemical level under the same conditions for all oligomers (for instance with the same symmetry restrictions) to perform a reliable extrapolation. Most of the quantum-chemical approaches used to compute transition energies are indeed very sensitive to the nature of the input geometries, and significant changes can be observed when optimizing geometries at different theoretical levels, or even with different parameterizations of a semiempirical approach. Moreover, the molecular backbones should be forced to be planar for B-type molecules, i.e., where a planar equilibrium geometry is expected, see Section 2.1. As a matter of fact, because the potential energy hypersurfaces are very flat with respect to the torsional degrees of freedom for these molecules, the determination of the geometric structure associated to the absolute minimum is a delicate issue: A lack of careful examination of the results can lead to large deviations in the calculated transition energies, and to changes in the $1/N$ plots, in an unpredictable manner (see Section 4).

2.3. Substitution Effects

Substituents attached to the molecular backbone can significantly shift the adiabatic S_0–S_1 electronic transition of oligomers to lower energies, with a shift ranging from –0.05 to –0.3 eV (and down to –1.5 eV in the extreme case of short oligomers with push–pull substituents). This shift is triggered by the mesomeric (±M, with + and – indicating a donor and acceptor effect, respectively) and/or inductive (±I) effects associated with the substituents, leading to an asymmetric (de)stabilization of the highest occupied molecular orbital (HOMO) and lowest unoccupied molecular orbital (LUMO) levels. A striking exception is substitution with fluorine atoms, in which case the subtle balance between the +M and –I effects leads to either a blue- or red-shift, depending on the number and position of the substituents[75] as well the nature of the molecular backbone.[75–77]

A red-shift of the adiabatic transition energy upon substitution does not necessarily imply a red-shift of the vertical transition energy and of the absorption maximum (A_{max}), because the latter are also influenced by the shape of the torsional potential in the electronic ground state. This is clearly evidenced by regioregular oligo(3-octylthiophenes), in which F_1 is red-shifted compared to the unsubstituted nT species, while A_{max} is blue-shifted. This points to a strongly modified double-well potential in the electronic ground state, which is effectively less steep than those of the unsubstituted nT (see Fig. 9). In general, the bathochromic shift of the adiabatic transition upon substitution slightly decreases with increasing chain length (Fig. 9). This suggests that the impact of the ±M and/or ±I effects of the substituents on the electronic structure is more pronounced in small oligomers.

When the substituents are exclusively attached to the external rings, the impact of the substituents is pronounced only in the shortest oligomers; the bathochromic shift decreases monotonously with chain size, vanishing at ca. $n \geq 8$ (see also Section 4).[78] Compounds with donor–acceptor substituents at the terminal positions exhibit a large bathochromic shift, which results from intramolecular charge transfer (see Fig. 10).[50] The amplitude of the transferred charge is reduced when the size of the interjacent conjugated backbone is elongated. For some compounds, the push–pull effect is so pronounced that it overcompensates the usual bathochromic shift observed with an increase in chain size (see Fig. 10).[50] The Kuhn model (Eq. 8) cannot account for this effect, because it neglects the role played by intramolecular charge-transfer processes. In this case, we suggest the use of a combination of the Kuhn expression and an exponential term, resulting in a four-parameter fit that is written as

$$E = E_0 \sqrt{1 + 2\frac{k'}{k_0}\cos\frac{\pi}{N+1}} - A \cdot \mathrm{e}^{-\mathrm{b}N} \qquad (9)$$

Equation 9 provides a good fit to the experimental values if E_{00} and k'/k_0 are adjusted to the monosubstituted species

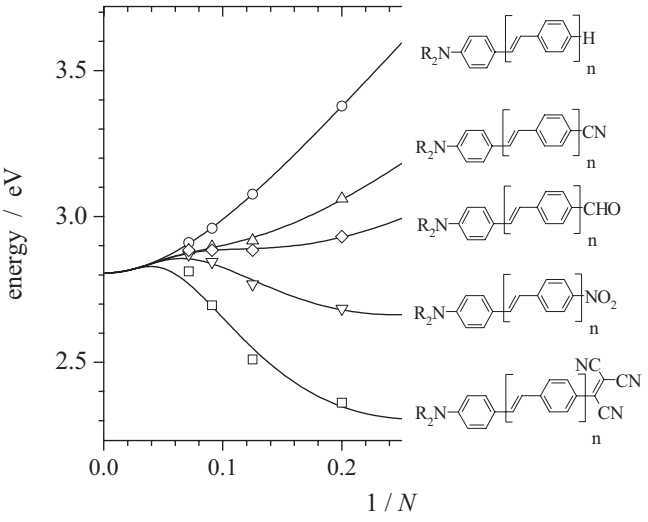

Figure 10. Spectral positions of the absorption maxima of terminally push–pull substituted oligo(phenylene vinylene)s in $CHCl_3$ [50]. Lines are modified Kuhn fits to the oligomer values according to Equation 9.

(dialkylamino-nPVs), to account for the convergence of the optical properties of the different oligomer series for large values of N.

2.4. Solvent Shifts

Because theoretical calculations are usually performed in the gas phase, whereas most UV-vis experiments are carried out in solution, the solvent effect is a critical issue when comparing theoretical and experimental results. Solvent shifts can be as large as 0.3 eV for optically allowed transitions, even in nonpolar solvents where specific solute–solvent interactions are not expected.[9,12,79] For most of the molecules under consideration in the present review, gas-phase data are not available because of their low vapor pressure. A possible approach to experimentally evaluate solvent shifts relies on the Onsager model, which is based on a reaction-field model involving a spherical cavity.[80] In this framework, the solvent shift (in eV) in a polarizable nonpolar medium is expressed as

$$E - E_{vac} = -329.2 \cdot \frac{f_{vac}}{R_0^3 \cdot E_{vac}} \cdot \frac{n^2 - 1}{2n^2 + 1} \qquad (10)$$

where n is the refractive index at the energy of the electronic transition, E_{vac} is the transition energy, f_{vac} is the oscillator strength in vacuum, and R_0 is the effective radius of the cavity (in Å).

Although in most cases the choice of a spherical cavity is clearly a strong approximation, Equation 10 works very well when used as a fitting function to estimate the transition energies in vacuum. This is illustrated for quinquethiophene in Figure 11, where the transition energies associated to F_1 in different solvents are plotted as a function of the Onsager

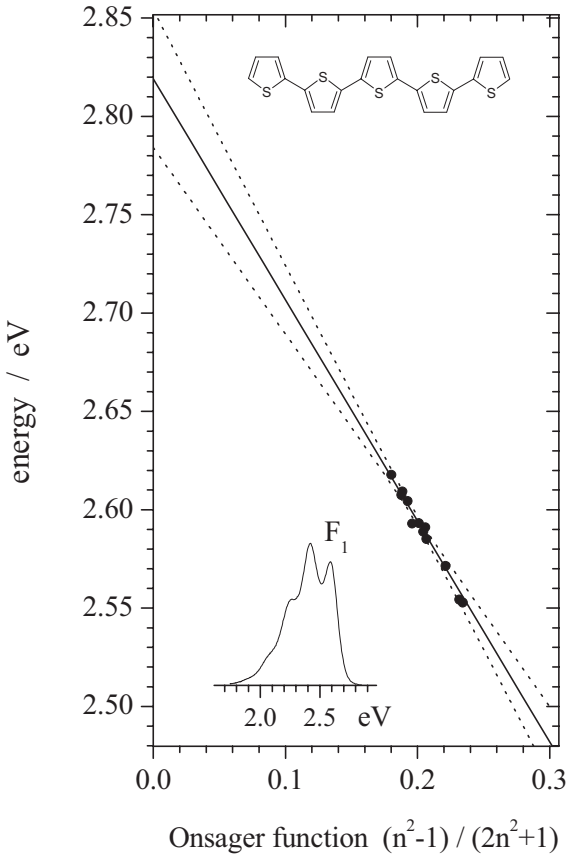

Figure 11. Experimental spectral positions of adiabatic transition energies (estimated as the F_1 positions, see inset) of quinquethiophene (chemical structure on top) as a function of the Onsager expression featuring the refractive index n_{solv} in a series of saturated hydrocarbon solvents [12]. The abscissa is scaled according to the Onsager relation. Solid line: linear fit. Dashed lines: 95 % confidence bands.

model (Eq. 10). The corresponding value in vacuum, with a standard deviation of ±0.02 eV, is obtained by linear extrapolation. It is also worth noting that temperature-induced spectral shifts are mainly a result of changes in the polarizability, induced by variations in the density of the solvent,[12] and only to a small extent a result of the planarization of the molecular backbone, which sum up to ca. 0.01–0.02 eV.[9] Furthermore, "bad solvents" or the lowering of temperature might lead to spontaneous aggregation with the formation of suspended nanometer-sized solid particles, as described elsewhere.[11,81,82] The subsequent spectral shifts of the optical spectra will be discussed in Section 2.5, which describes solid-state effects. At the theoretical level, formalisms to deal with solvent effects are implemented in several quantum-chemical packages, on the basis of dielectric continuum models of growing complexity (going from spherical cavities to cavity shapes adapted to the molecules).[83] Specific solvent interactions in polar media that may significantly alter the spectral shapes are more difficult to treat.[84]

2.5. Solid-State Effects

Further complications arise when comparing transition energies calculated for isolated systems with experimental data in the condensed phase (e.g., vapor-deposited films, crystallites, or nanoparticle suspensions), because optical properties are also strongly affected by intermolecular interactions in the solid state. The shape of the spectra in the solid state depends on the optical characteristics of the isolated molecules (transition energies and associated oscillator strengths), and on their relative arrangement (in particular the intermolecular distances and the rotational angles between their long molecular axes). The spectral shapes can be further modulated by coupling with intermolecular vibronic modes.[17] In view of the large variety of spectral changes observed experimentally, an estimation of the amplitude of solid-state effects is of paramount importance but not straightforward, in particular for insoluble materials such as unsubstituted π-conjugated polymers.

In general, the electronic interactions between molecules take place in the weak to medium coupling regime. Electronic excitations are collective (i.e., delocalized over several chains) and induce strong changes in the shape of the absorption spectra, compared to the isolated molecules. This is particularly the case when the transition dipole moments of the molecules are parallel, leading to the formation of so-called H-aggregates, characterized by strongly blue-shifted absorption spectra.[17,85] However, self-trapping of the collective excitations upon nuclear relaxation in the excited states leads to localized emission processes. When intermolecular vibronic modes do not alter the emission characteristics, the shape of the emission spectrum is similar in the solid state and in solution.[17] This implies that the adiabatic transition energies can be determined from the F_1 positions measured in the solid state, and used to assess the amplitude of the spectral shifts induced by intermolecular effects (Fig. 12). Note that planarization of the molecular backbones, which is a typical side-effect of solid-state organization, might also induce slight spectral shifts (Sec. 2.4); however, in general they are small compared to the significant bathochromic shifts, up to 0.3 eV, induced by intermolecular effects (see Section 3.5).

3. Experimental Results

In order to quantify the various effects described in Section 2, illustrative examples are given hereafter. As mentioned in the introductory paragraph, the examples have been selected to illustrate the previous concepts rather than to offer a full quantitative analysis of substitution, solvent, solid-state, and temperature effects for a large variety of materials. We focus here on oligophenylenes (*n*P), oligo(phenylene vinylene)s (*n*PV), and oligothiophenes (*n*T) of different sizes and substitution patterns to investigate the different effects.

ADVANCED MATERIALS

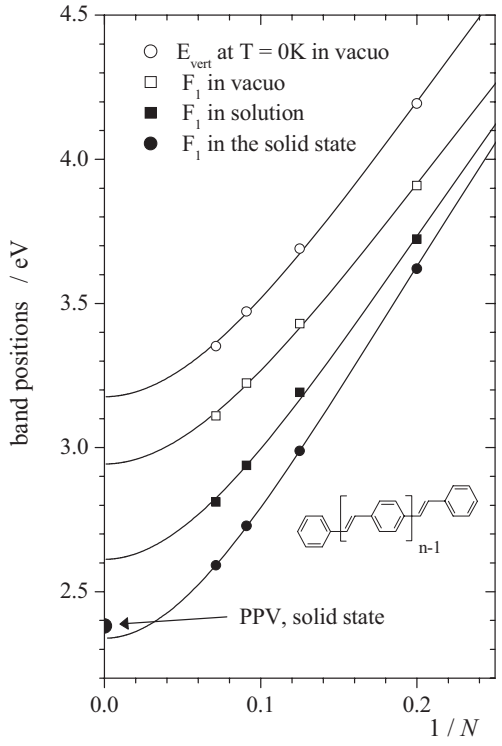

Figure 12. Electronic transitions of oligo(phenylene vinylene)s *n*PV (n=1–4) [9]. ○: Vertical transition energies E_{vert} at $T \rightarrow 0$ K according to Equations 2a and 4 extrapolated to vacuo with Equation 10. □: F_1 positions extrapolated to vacuo. ■: F_1 positions in solution (dioxane). ●: F_1 positions in *n*PV based nanoparticles and in a PPV film [10]. Solid lines are Kuhn fits to the oligomer values according to Equation 8.

3.1. Chain-Length Dependence

The chain-length dependence of the transition energies of the oligomers has been fitted with Equation 8, with E_0 and $g = k'/k_0$ taken as tunable parameters. A first approach to judge the quality of the extrapolation procedure is to focus on very long oligomers. The fit performed in Figure 6 for the alkyl-substituted oligothiophenes containing up to 96 rings is reasonably good, although a slightly smaller gradient is experimentally observed for large values of N. The extrapolation procedure can be tested further by comparing the results with available polymer values, as long as the same experimental conditions (in terms of substitution pattern, temperature, and solvent) are used for both the polymer and the corresponding oligomers. Such a comparison cannot be made with unsubstituted molecules, because of the insolubility of the parent polymers. In the case of substituted polymers, the agreement between the extrapolated and experimental polymer values is good: deviations by less than 0.03 eV (corresponding to an error of less than 1 %) are obtained for alkoxy-substituted *n*PVs (Table 2), L*n*Ps (Fig. 8), and regioregular octyl-*n*Ts (Fig. 9). It should be emphasized that the difference between a fit based on Equation 8 and a linear fit is not negligible, being typically around 0.3 eV (this is equivalent to 10–15 % of the absolute value of the polymer optical bandgap). While the fitting procedure based on Equation 8 works well for most of the oligomers under study, a good fit of the adiabatic transition energies is possible only for $n > 2$ for unsubstituted oligophenylenes *n*P (see also Sec. 4.1). This is explained by the fact that the emission originates from a symmetry-forbidden state in 2P,[7,23] while the lowest excited state is optically allowed in longer *n*P oligomers as well as *n*PV and *n*T oligomers.

3.2. Equilibration Energies

The equilibration energies associated to the emission (ΔE_{eq}(em)) are reported in Figure 7 for oligothiophenes of different sizes, as determined from the emission spectra on the basis of Equation 2. The value of ΔE_{eq}(em) decreases with the number of repeat units, owing to the fact that the amplitude of the geometric changes over the molecular backbone reduces with chain size. Fitting the $1/N$ dependence by Equation 8 yields an estimate of the equilibration energy at the polymer limit of 0.21 eV for polythiophene (PT) (see Fig. 7). In polyphenylene (PP), the equilibration energy ΔE_{eq}(em) amounts to 0.18 eV (Table 1), indicating that upon nuclear relaxation smaller geometric deformations take place in PP than in PT. This is primarily rationalized by the fact that benzene rings are more aromatic (higher resonance energy) than thiophene rings, and are thus less subject to geometric distortion. The introduction of vinylene units between aromatic rings softens the geometry of the chain, and promotes larger equilibration energies (the ΔE_{eq}(em) of PPV is 0.23 eV, cf. Fig. 12 and Table 1).

The equilibration energies, extracted from absorption spectra at room temperature by using Equation 2a, are much larger, because of the thermal excitation of low-frequency torsional modes: ΔE_{eq}(abs) = 0.36 eV for PT while for emission ΔE_{eq}(em) = 0.21 eV (see Fig. 7). The contribution of thermal activation to the equilibrium energy (see Eq. 5), is estimated to be ΔE_{th} = 0.15 eV for PT and 0.05 eV for PPV. In PP, the equilibration energy becomes as large as 0.57 eV (Table 1). This value reflects the presence of a nonplanar equilibrium geometry in the ground state (C-type character).

Substituents do not substantially impact the geometry relaxation associated to the emission process (see Table 2). However, the substitution effects can become significant for the absorption process at elevated temperatures, because they significantly alter the ground-state torsional potential. This is the case for oligo(3-octylthiophenes), for which the equilibration energy for absorption becomes as large as 0.59 eV at the polymer limit (see Fig. 9).

3.3. Substitution Effects

Alkyl and alkoxy substitution on the rings leads to an overall decrease of the adiabatic transition energies,[81] cf. the ΔE_{sub} values in Table 2. The corresponding bathochromic shift is reduced with increasing chain length (Fig. 9), thus indicating that the changes in the electronic structure of the molecular backbones by the inductive and mesomeric effects of the substituents are

Table 2. Optical properties of substituted polymers determined by the oligomer approach from experimental values (in eV): Spectral positions of F_1, shifts upon substitution ΔE_{sub} in comparison to the unsubstituted polymer chain (see Table 1). The experimental adiabatic transition energies of the polymers in solution and in the solid state are also given in the last columns.

		Oligomer approach					Polymer			
Compound	Structure	Substituents	Maximum *n*	Solvent	$E(F_1)$ [eV]	ΔE_{sub} [eV]	Substituents	E_{00} solution [eV]	E_{00} solid state [eV]	ΔE_{cryst} [eV]
LPP	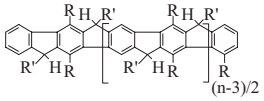	R = C_6H_{13} R' = Ph-$C_{10}H_{21}$	7 [a]	CH_2Cl_2	2.75	–0.20	R = C_6H_{13} R' = Ph-$C_{10}H_{21}$ [a]	2.76	2.68	0.09
RO-PPV	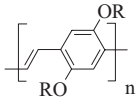	R = C_3H_7 R = O-*iso*C_5H_{11}	8 [b] 6 [d]	CH_2Cl_2 $CHCl_3$ [e]	2.32 2.26	–0.26 –0.32	MeH [c] R = O-isoC$_5H_{11}$ [f]	2.23 2.24	2.16 2.07	0.07 0.17
P3RT	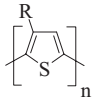	R = C_8H_{17}	6 [g]	$CHCl_3$	2.14	–0.09	rr-Oct [g] rr-Hex [h] rra-Hex [h]	2.14 2.12 2.18	1.91 2.08	0.21 0.10
	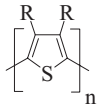	R, R = 	96 [i]	THF	2.10	–0.12				
PEDOT	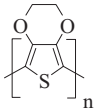		4 [j]	CH_2Cl_2	1.95	–0.29		–	1.64 [k]	–

[a] See Grimme et al., F_1 positions [16]. [b] See Oelkrug et al. [86]. [c] See Gaab et al., F_1 positions [87]. [d] See Peeters et al., [88]. [e] Low-temperature value. [f] See Chiavarone et al., F_1 positions [10]. [g] See Bras et al. and Bidan et al. [32, 33]. [h] See Gierschner et al. [89]. [i] See Otsubo and co-workers [46]. [j] See Apperloo et al. [90]. [k] See Havinga et al. and Dietrich et al. [91, 92].

attenuated with chain size, in agreement with quantum-chemical calculations.[39] Comparison of PT with its regioregular hexyl-substituted analogue rr-P3HT yields a substituent shift ΔE_{sub} of –0.09 eV. The substitution of each ring by several alkyl chains induces a slightly enhanced bathochromic shift, compared to the oligomers bearing a single substituent per ring. Analysis of the data collected in Table 2 further indicates that the inductive effects are rather insensitive to the exact nature of the molecular backbone. The substitution with alkoxy groups leads to larger red-shifts compared to alkyl substituents, resulting from the introduction of a mesomeric effect associated to the oxygen atoms. This translates into a ΔE_{sub} value of –0.29 eV for PT. The impact of such a mesomeric effect does not appear to be affected by the nature of the molecular backbone, as evidenced for the alkoxy-substituted PPV and PT derivatives in Table 2. It is worth noting that this trend might not hold true for polymers featuring an alternation of donor versus acceptor units.

3.4. Solvent Shifts

The experimental determination of solvent effects for polymers via the oligomer approach is lengthy, because the solvent shifts have to be determined for each oligomer. To maximize the accuracy of the extrapolation method based on Equation 10, a rather large number of solvents has to be considered (see Fig. 11). The nature of the solvents should be similar enough to allow comparison (e.g., saturated hydrocarbons), but different enough to provide a large range of refractive indices (e.g., by varying the chain lengths). The typical shifts are on the order of 0.1–0.3 eV, and increase with the size of the conjugated backbones. The shift ΔE_{solv} is –0.32 eV for PPV (see Fig. 12) and is somewhat smaller for PT (ΔE_{solv} = –0.26 eV), because of the smaller oscillator strengths of *n*Ts compared to *n*PVs of similar effective radius (R_0), cf. Equation 10.

3.5. Solid-State Shifts

As discussed in Section 2.5, the spectral shifts ΔE_{cryst} induced in the solid state can be obtained from measurements of the position of the emission band in crystalline materials, thin films, or nanoparticles. However, the F_1 position might be altered by reabsorption effects[93] and by chemical contaminants, introducing trap states that can be populated via energy transfer.[94] Therefore, it is necessary to use very thin samples to extract reliable solid-state shifts, and to work under very clean conditions. Nanoparticles, obtained by fast pre-

cipitation from solvent mixtures, fulfill these conditions.[81] Moreover, a relevant extrapolation further requires that the oligomers and the parent polymer exhibit the same crystal packing. This is the case for unsubstituted *n*Ts and *n*PVs, which are organized in a highly anisotropic herringbone arrangement.[95,96] The crystal shift ΔE_{cryst} increases with the number of repeat units (see Fig. 12), and reaches values of –0.27 eV for PPV and –0.32 eV for PT (see Table 1). The actual experimental values for the polymers are smaller by ca. 0.08 eV, and point to the introduction of some disorder in the polymers. This is further reflected by considering *t*-butyl-substituted oligo(phenylene vinylene)s (B*n*PVs) whose bulky substituents prevent the formation of well-ordered structures.[17] In this case, the extrapolation of the spectral positions results in a crystal shift of –0.17 eV, which is significantly smaller than the value derived for the unsubstituted oligomers (see Table 1). We emphasize that these values must be treated with caution, in view of the rather small number of crystalline structures available for oligomers and the uncertainties in the determination of spectral positions in solid-state samples.

For polymers substituted by soluble side-chains, the crystal shifts can be directly inferred from the experimental data (see Table 2). The values of these shifts are remarkably smaller than the shifts of the corresponding unsubstituted polymers. This might be attributed to i) a smaller effective conjugation length in the substituted polymers, resulting from the larger steric effects induced by the substituents; ii) a reduction in the strength of the intermolecular interactions going from the herringbone packing, favored by unsubstituted polymers,[97] to the (shifted) face-to-face arrangements induced by the presence of the substituents;[98,99] and iii) on average, a larger intermolecular separation induced by the substituents ("side-chain dilution"). Such effects can be quantified by comparing the optical properties of regioregular (rr) and regiorandom (rra) hexyl-substituted polythiophene (P3HT, Fig. 13), because the steric effects in rra-P3HT are much larger than in rr-P3HT. The steric effects lead to a smaller optical bandgap (by –0.06 eV) for rr-P3HT in solution (see Table 2). The difference becomes larger in the solid state (–0.17 eV), because the orientation of the side-chains in rra-P3HT does not only induce a deviation of the polymer backbone from planarity, but also prohibits the dense and ordered packing of the chains, which prevails for rr-P3HT.[98] The difference between these two values (0.11 eV) yields a direct measure of the effect of disorder on the solid-state optical bandgap, in good agreement with the value obtained for disordered versus ordered PPV chains (0.10 eV, see Table 1).

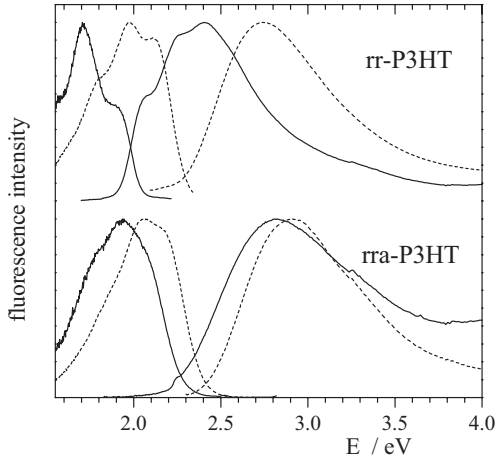

Figure 13. Fluorescence emission (left) and excitation (right) spectra of regio-regular (rr, top) and region-random (rra, bottom) poly-hexylthiophene chains (P3HT) in solution ($CHCl_3$, dashed lines), and in the solid state (nanoparticle suspensions, solid lines).

4. Theoretical Calculations

All effects discussed above have a large influence when transition energies calculated in gas phase are compared to experimental values. The errors can sum up to a value larger than 1 eV, i.e., about 50 % of the calculated energies, see Table 3. To provide reliable estimates of the optical bandgap of polymers, quantum-chemical methods must yield an accurate description of:

- the absolute energy of the electronic transitions
- the chain-size evolution
- the geometry/symmetry of the molecules
- the substitution effects
- the solvent (and temperature) induced shifts for polymers in solution
- the solid-state effects in crystalline materials, thin films, or nanoparticles.
- the potential hypersurface of the excited state to calculate vertical transition energies.

Moreover, a proper extrapolation procedure recommends the use of a rather large number of oligomers to improve the accuracy of the fit, and an accurate fitting function, for example, Equations 8 and 9.

In the following, the reliability of widespread quantum-chemical methods in predicting optical bandgaps at the polymer limit, with respect to the criteria listed above, is tested. The choice of the methods considered here is guided by their computational costs for large systems and the availability of literature data. Accordingly, we focus on semiempirical and ab initio Hartree–Fock methods coupled to a CIS scheme, as well as on the time-dependent density functional theory

Table 3. Maximum error sources (in eV) in determining the optical bandgap of polymers.

Effect	PPV	PT
Adiabatic vs. vertical transition	–0.28	–0.36
Substitution effect	–0.26	–0.29
Solvent effect	–0.32	–0.26
Solid-state effect	–0.27	–0.32
Σ	–1.13 (44 %)	–1.23 (56 %)

(TD-DFT) formalism. We emphasize that the introduction of at least doubly excited configurations in the configuration interaction (CI) expansion is required in some instances to properly describe excited states. This is the case, for instance, for the $2A_g$ state in polyenes, which lies below the $1B_u$ excited state, a feature that cannot be reproduced at the single CI level.[100–102] Such highly correlated states are also, in general, poorly described at the TD-DFT level. In contrast, the lowest optically allowed excited state of conjugated chains, which is the prime focus of this Review, is generally well described by these techniques. The choice of the active space in such calculations affects both the absolute transition energies and the slope in the $1/N$ representation. When a full active space is not used, it is important that the number of configurations scales with the size of the oligomers to yield reliable chain-size evolutions.

In standard approaches, both the TD-DFT and CIS calculations are performed in the gas phase at $T = 0$ K. A full comparison with experiment would thus require the solvent effects to be taken into account, either by the experimental method described in Section 2.4 or by their explicit treatment in the quantum-chemical calculations.[103] Unfortunately, the most sophisticated solvent models are not yet available for all quantum-chemical approaches, so that the experimental method is generally preferred. Note that the semiempirical ZINDO method is parameterized to reproduce experimental vertical transition energies in solution. A direct comparison of the calculated values with experimental data in solution is generally achieved, because changes linked to variations in the refractive index among "standard" solvents such as hexane or chloroform are smaller than the errors of semiempirical methods.

4.1. Ab Initio Hartree–Fock RCIS

The left part of Figure 14 compares the experimental $S_0 \rightarrow S_1$ vertical transition energies E_{vert} of *n*PVs in vacuo, as obtained by the extrapolation method given by Equation 10, with Hartree–Fock calculations for different basis sets coupled to a CIS scheme. The direct evaluation of E_{vert}, as obtained from a single-point calculation at the S_0 geometry, largely overestimates the experimental values in vacuo by about 1 eV.[71]

The agreement with experiment is improved when comparing the adiabatic transition energies E_{00} by relaxing the excited-state geometry in the calculations (Fig. 14). Much better results are obtained when large basis sets are used; the 6-311G* basis set gives a high accuracy of ca. 0.03 eV, equivalent to an error of ca. 1 %.[9] Geometric constraints supported by experimental results[9] (for instance imposing a planar conformation with a C_{2h} symmetry) are essential to yield a correct description of the chain-length dependence. The absence of such constraints would allow for a random walk on the very flat potential hyper-surface in the ground state, which in turn would produce rather random numbers for E_{00}. This might lead to a situation where the transition energy increases with increasing chain length for large values of N,[71] in stark contrast with the experimental results (see Fig. 14).

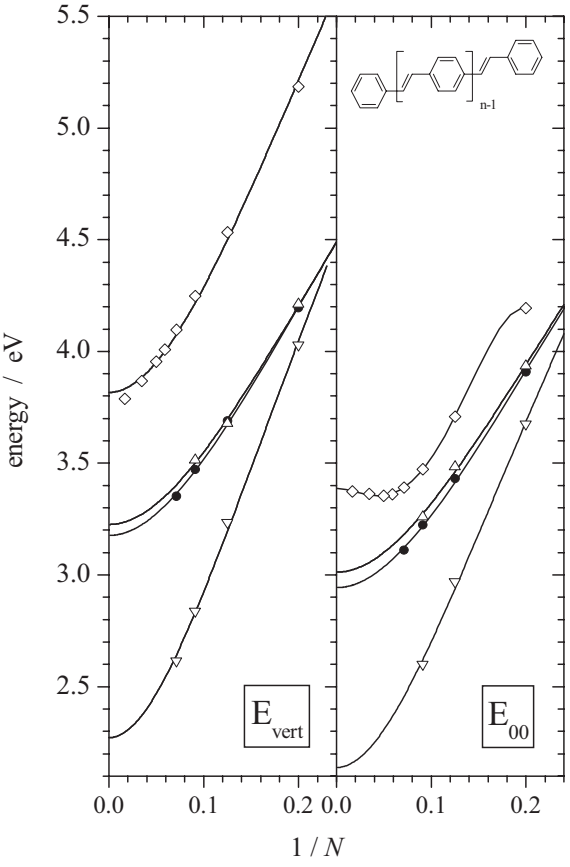

Fig. 14: Vertical (E_{vert}, left) and adiabatic (E_{00}, right) transition energies of *n*PVs. Left: Experimental values in vacuo (●) [9]. Hartree–Fock (HF) calculations with different basis sets and methods: RCIS/3-21G* with C_{2h} symmetry (◇) [71], RCIS/6-311G* with C_{2h} symmetry and geometry optimization in the S_1 state to use Equations 2a and 6 (△), [9]. TD-DFT calculation (B3LYP/6-31G*, ▽) [19]. Solid lines are Kuhn fits to the experimental and calculated values. Right: Experimental values in vacuo (●) [9], Kuhn fits (solid lines). HF calculations with different basis sets and methods: RCIS/3-21G* without symmetry restriction (◇, solid line: 4th order polynomic fit) [71], RCIS/6-311G* with C_{2h} symmetry restriction (△) [9]. TD-DFT calculation (B3LYP/6-311G*, ▽) [104].

The vertical transition energies, obtained from E_{00} together with an explicit calculation of the equilibrium energy ΔE_{eq} via Equation 6, show a very good agreement with experiment. This points to a correct description of the excited-state geometry by the RCIS method (Fig. 14).[9] A similar accuracy is obtained for E_{00} and E_{vert} for oligothiophenes *n*T, as long as diffuse functions are included in the basis set to better describe the sulfur atoms (see Fig. 15).[12] The increase in the vertical transition energy E_{vert}(abs) with temperature, caused by thermal excitation of low-frequency modes, is well reproduced by theory from a model based on undisplaced distorted oscillators (Fig. 2) with the correct torsional frequencies in the S_0 and S_1 state used as input parameters and the vibrational lev-

ADVANCED MATERIALS

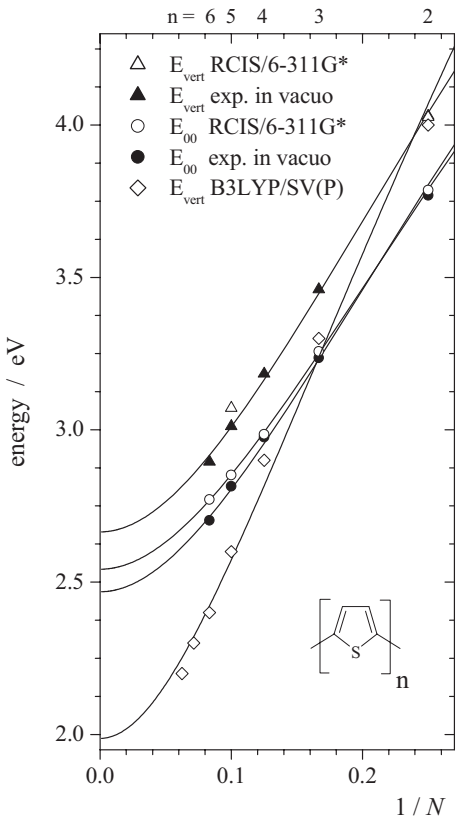

Figure 15. Vertical (E_{vert}) and adiabatic (E_{00}) transition energies of *n*Ts. Experimental E_{vert} (▲) and E_{00} (●, [12]) in vacuo, as obtained by Equation 10. HF RCIS/6-311+G* with geometry optimization of the S_1 state and C_{2h} symmetry restriction [12]. E_{00} (○), E_{vert} (△), obtained from Equations 2a and 6. TD-DFT B3 LYP/SV(P) calculations of E_{vert} (◇, [111]). Solid lines are Kuhn fits to the experimental and calculated values.

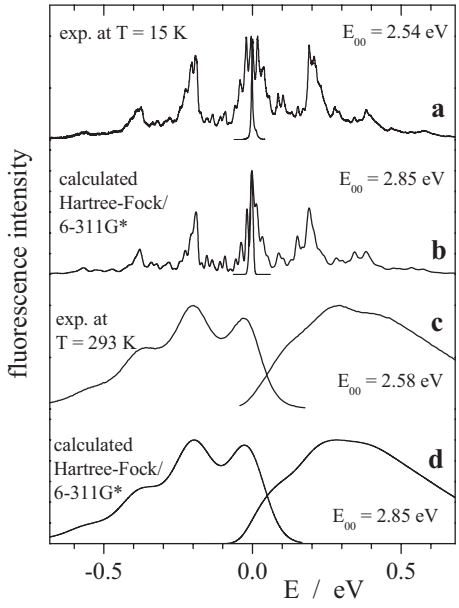

Figure 16. Experimental (in tetradecane) and calculated fluorescence emission (left) and excitation (right) spectra of quinquethiophene (5T), [12]. From top to bottom: a) Experimental spectra at 15 K. b) Calculated spectra (HF CIS/6-311G*, vibrational frequencies DFT B3LYP/6-311G*, broadening of the spectra with a Gaussian function with a half-width of 130 cm^{-1}). c) Experimental spectra at 293 K. d) Calculated spectra (Gaussian half-width of 1100 cm^{-1}, with thermal excitation of torsional modes as calculated at the DFT B3LYP/6-311G* level, [104]).

els populated via a Boltzmann distribution.[9] However, it has to be kept in mind that the vibrational frequencies are systematically overestimated by Hartree–Fock methods.[105] A hybrid approach that takes the frequencies from DFT-based calculations yields a better agreement with experiment, and reproduces not only the experimental spectra at low temperature but also translates into the increase in E_{vert}(abs) with temperature (see Fig. 16). A perfect match between the experimental and theoretical spectra is generally not observed, because of large errors in the estimates of the energies of the low-frequency modes ($\nu < 100$ cm^{-1}).

For *n*Ps, no experimental value in vacuo for $n > 2$ is available; however, only small blue-shifts on the order of 0.05–0.15 eV with respect to the values in solution (Fig. 17) are expected, in view of the rather small oscillator strengths and high electronic transition energies of these oligomers (see Eq. 10). On that basis, the E_{00} values, calculated by RCIS, are found to be in good agreement with experiment, except for biphenyl (2P), because the lowest excited state is forbidden in 2P (the intersection between the experimental absorption and emission spectra is well below the E_{00} value of the optically allowed transition, see Fig. 17).

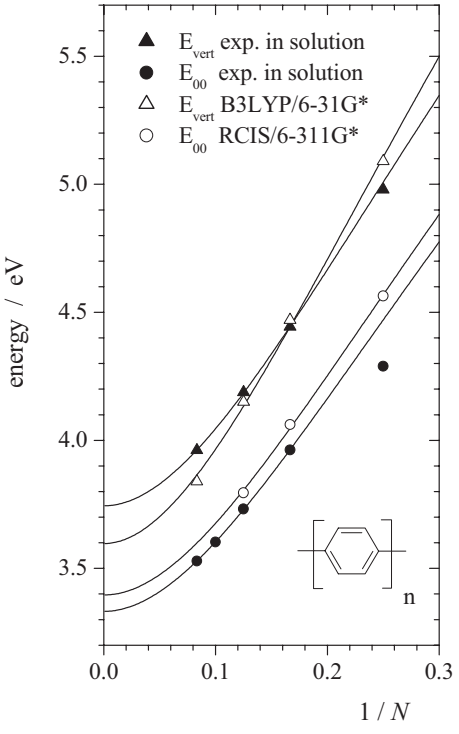

Figure 17. Experimental vertical (E_{vert}, ▲) and adiabatic (E_{00}, determined as the intersection of the absorption and fluorescence spectra, ●) transition energies of *n*Ps in cyclohexane [23]. Calculated E_{vert} at the TD-DFT level of theory without geometry constraints (B3LYP/6-31G*, △, [19]). Calculated E_{00} at the HF RCIS/6-311G* level (geometry D_{2h}, ○, [106]).

Although the RCIS method proves very successful to estimate the electronic transitions of the systems under study, several limiting factors should be mentioned: i) RCIS calculations are time-consuming, because they require geometry optimizations of the lowest excited state; and ii) experimental shifts induced by substituents are only partly reproduced (Fig. 18), in particular, the strong bathochromic shift induced by the push–pull substituents in Figure 19 appears to be largely underestimated in the shortest oligomers.

4.2. Time-Dependent Density Functional Theory

The high accuracy of DFT methods in predicting molecular geometries and vibrational frequencies encouraged numerous groups to calculate electronic transitions at the TD-DFT level. The comparison of the vertical and adiabatic transition energies calculated for *n*PVs (Fig. 14), *n*Ts (Fig. 15), and *n*Ps (Fig. 17) with the experimental values in vacuo reveals a strong overestimation of the slope in the 1/*N* representation, resulting from the overestimation of long-range electron correlation effects in the TD-DFT methods.[72] A reliable prediction of the polymer properties from *n*PVs (Fig. 14) as well as for other oligomer series such as *n*Ts (Fig. 15), *n*Ps (Fig. 17),[108] *n*TVs[109] or oligoacenes[110] with standard DFT approaches cannot therefore be accessed, whatever the functional (B3LYP,[19,30,34–36,111–114] BP86,[34,110] B3P86-30 %,[5,36] BLYP,[34,110] SVMN,[19] PB1PBE,[19] LSDA[36]) or the basis set.[34] Hybrid methods in which the TD-DFT formalism is applied to ground-state geometries optimized at the Hartree–Fock level lead to an overall shift of the calculated transition energies[39] while keeping the overestimated slope in the 1/*N* representation.

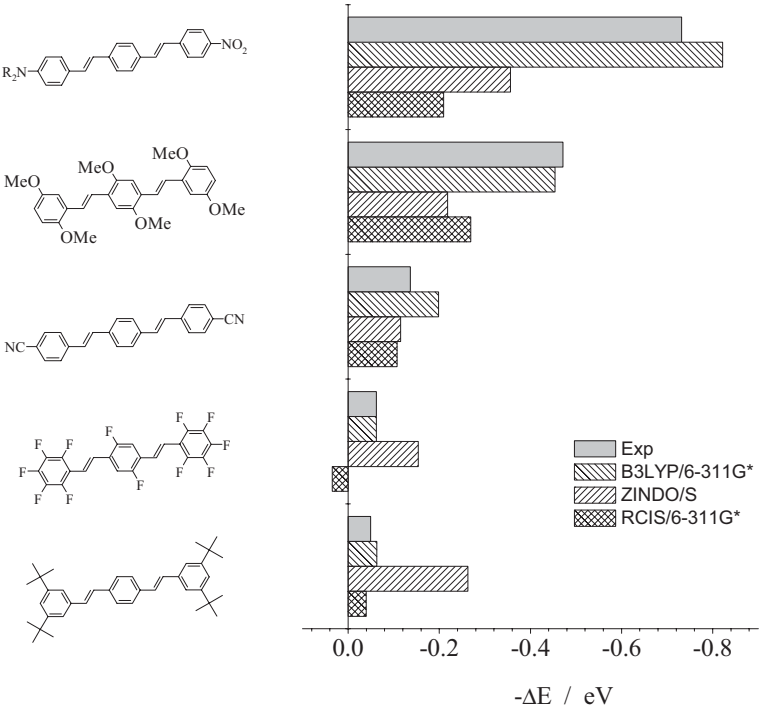

Figure 18. Shifts of the lowest optical transition of substituted distyrylbenzenes (2PV) with respect to the unsubstituted molecule. Experimental values in hexane [17,50,81,107], calculated values with an imposed C_{2h} symmetry at the TD-DFT B3LYP/6-311G*, ZINDO/S, and HF RCIS/6-311G* levels.

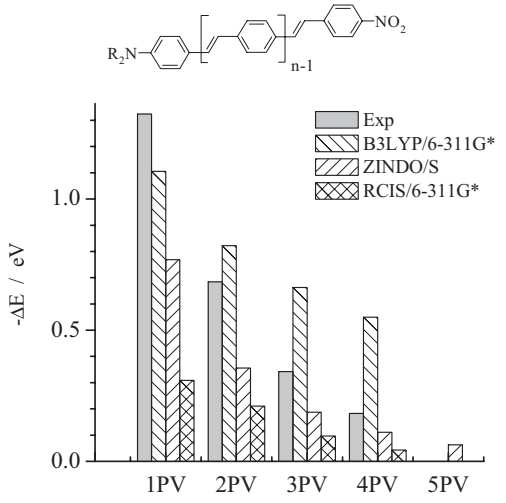

Figure 19. Bathochromic shifts of *p*-nitro,*p'*-dialkylamino-substituted OPVs with respect to the unsubstituted oligomers. Experimental values of absorption maxima in $CHCl_3$ [50], calculated values at the TD-DFT B3LYP/6-311G*, ZINDO/S, and HF RCIS/6-311G* levels.

For small molecules, the impact of inductive and/or mesomeric effects induced by substituents appear to be very well reproduced (Fig. 18); however, the agreement with the corresponding experimental values deteriorates when the chain size is increased (Fig. 19). The general overestimation of long-range electron correlation effects also shows up, albeit to a much smaller extent, in the estimates of equilibration energies, which tend to be underestimated by the TD-DFT method (the deviation with respect to the experimental values increases with *N*).[104] In view of these restrictions, TD-DFT methods have a limited range of applicability in their present form.

4.3. Semiempirical Methods

A good compromise between computational time and accuracy is offered by semiempirical methods. The most popular method for the prediction of vertical transitions of π-conjugated molecules is ZINDO based on geometries optimized at the semiempirical Hartree–Fock AM1 (Austin model 1) or PM3 (parameterized method 3) levels, or at the DFT level. Figure 20 compares the ZINDO/S results obtained for *n*Ps, *n*PVs, and *n*Ts in a consistent manner. All geometry optimizations are performed with the AM1 method within the AMPAC package,[115] using planar geometries (fully relaxed nonplanar geometries are also considered for

ADVANCED MATERIALS

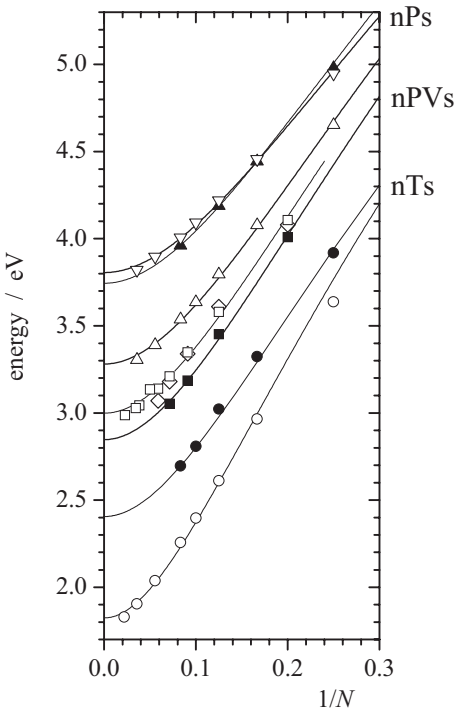

Figure 20. Experimental vertical transition energies E_{vert} of *n*Ps (▲, in hexane), *n*PVs (■, in dioxane), and *n*Ts (●, in CH_2Cl_2). Calculated E_{vert} at the ZINDO/S level with a CI active space encompassing all occupied and unoccupied π-type orbitals on the basis of AM1-optimized geometries: *n*Ps (nonplanar: △, planar: ▽), *n*PVs: (□, planar), *n*Ts: (○, planar). Calculated E_{vert} of *n*PVs at the AM1/CAS level (◇, [69]).

*n*Ps). These calculations involve the complete set of π and π* orbitals. The agreement between the calculated transition energies and the corresponding experimental values obtained in nonpolar solvents is very satisfactory for *n*PVs and *n*Ps. The larger discrepancy observed for oligothiophenes can be attributed to the poor description of the C–C bond alternation in the thiophene rings given by AM1,[116] and/or a deficient parameterization of sulphur in ZINDO. The mesomeric and/or inductive effects induced by substituents also appear to be underestimated at the ZINDO level (Figs. 18 and 19). Calculations on the *n*PV series[117] performed at the AM1/CAS (compete active space) level also provide a good agreement with experiment for both vertical and adiabatic transition energies (Fig. 20).[117] However, the quality of the results depends somewhat on the nature of the molecules under study, as a less optimal agreement is obtained for *n*Ps.

5. Conclusions

The characterization of the optical properties of conjugated polymers via the oligomer approach requires a proper determination of the oligomer properties and relevant extrapolation procedures. A deep knowledge of the parameters that control optical bandgaps is another prerequisite to allow the comparison between experimental data and quantum-chemical calculations. In this Review, we first discussed the best strategies to extract the optical characteristics of conjugated oligomers from the absorption and emission spectra and relevant extrapolation procedures to reach the polymer limit. The impact of conformational effects, thermal excitations, variations in the substitution pattern, as well as solvent and solid-state effects were analyzed at the experimental level for different molecular backbones. Systems presenting different polarizabilities and flexibilities were selected, namely oligophenylenes, oligo(phenylene vinylenes), and oligothiophenes. If the different parameters affecting the optical bandgap are not considered in quantum-chemical calculations, deviations as large as 1.2 eV are expected with respect to corresponding experimental measurements. Incorrect extrapolation procedures (for instance linear extrapolations with respect to $1/N$) can generate errors as large as 0.3 eV.

By confronting experimental data to the results of standard quantum-chemical approaches, we were led to the conclusion that i) Hartree–Fock CIS methods give very reliable results for optically allowed singlet–singlet transitions, provided that the geometry of the excited state is optimized and that the basis set is rather large; ii) TD-DFT methods generally overestimate the chain-size evolution of the electronic transition energies, independent of the functional and basis set chosen; and iii) a good compromise between computational time and accuracy is obtained with semiempirical Hartree–Fock methods.

Received: February 10, 2006
Revised: April 5, 2006
Published online: January 3, 2007

Note added in proof: After the submission of this manuscript, two relevant papers on the subject have been published.[118, 119] In both papers, TD-DFT calculations on long oligothiophenes with up to 40 units were performed. Both studies confirm the saturation of the lowest transition energies for very long oligomers, in accordance with previous investigations (see Section 2.2); they also stress the different conditions for the calculations (single chains in the gas phase) and for the experiments (solid-state phase). While Salzner et al.[118] estimate the geometry relaxation, solvent, and solid-state effects, Zade and Bendikov[119] do not address their impact, thus claiming too fast an accurate prediction of the experimental optical gap; in addition, their B3LYP/6-31G* calculations yield a much too low value of 2.0 eV. The calculated transition energy obtained by Salzner et al.[118] for the polymer using the B3P86-30% functional ($E_{vert} = 2.5$ eV) is in much better agreement with experiment; however, this is a result of the fact that their calculated values for short oligomers are far too large. Thus, the strong overestimation of the slope in the $1/N$ representation with standard DFT methods, as stated in Section 4.2, also applies for these recent calculations.

[1] R. H. Friend, R. W. Gymer, A. B. Holmes, J. H. Burroughes, R. N. Marks, C. Taliani, D. D. C. Bradley, D. A. dos Santos, J. L. Brédas, M. Lögdlund, W. R. Salaneck, *Nature* **1999**, *397*, 121.

[2] M. Pope, C. E. Swenberg, *Electronic Processes in Organic Crystals and Polymers*, Oxford University Press, New York **1999**.
[3] *Electronic Materials: The Oligomer Approach* (Eds: K. Müllen, G. Wegner), Wiley-VCH, Weinheim, Germany **1998**.
[4] J.-L. Brédas, in *Handbook of Conducting Polymers* (Ed: T. A. Skotheim), Marcel Dekker, New York **1986**. pp. 859–913.
[5] U. Salzner, *Curr. Org. Chem.* **2004**, *8*, 569.
[6] B. E. Kohler, in *Conjugated Poymers* (Eds: J.-L. Brédas, R. Silbey), Kluwer, Dordrecht, The Netherlands **1991**, p. 405.
[7] F. Momicchioli, M. C. Bruni, I. Baraldi, *J. Phys. Chem.* **1972**, *76*, 3983.
[8] Y. Pelous, G. Froyer, C. Hérold, S. Lefrant, *Synth. Met.* **1989**, 29, E17.
[9] J. Gierschner, H.-G. Mack, L. Lüer, D. Oelkrug, *J. Chem. Phys.* **2002**, *116*, 8596.
[10] L. Chiavarone, M. Di Terlizzi, G. Scamarcio, F. Babudri, G. M. Farinola, F. Naso, *Appl. Phys. Lett.* **1999**, *75*, 2053.
[11] D. Oelkrug, H.-J. Egelhaaf, J. Gierschner, A. Tompert, *Synth. Met.* **1996**, *76*, 249.
[12] J. Gierschner, H.-G. Mack, H.-J. Egelhaaf, S. Schweizer, B. Doser, D. Oelkrug, *Synth. Met.* **2003**, *138*, 311.
[13] S. Hayashi, K. Kaneto, K. Yoshino, *Sol. State Commun.* **1987**, *61*, 249.
[14] In this article, we define the optical bandgap as the adiabatic transition energy. In contrast to inorganic semiconductors, the electronic transition energy is not identical to the HOMO–LUMO gap, but has to be corrected by electron correlation (see, for example, J. Michl, E. W. Thulstrup, *Tetrahedron* **1976**, *32*, 205).
[15] J. Roncali, *Chem. Rev.* **1997**, *97*, 173.
[16] J. Grimme, U. Scherf, *Macromol. Chem. Phys.* **1996**, *197*, 2297.
[17] J. Gierschner, M. Ehni, H.-J. Egelhaaf, B. Milián Medina, D. Beljonne, H. Benmansour, G. C. Bazan, *J. Chem. Phys.* **2005**, *123*, 144 914.
[18] M. I. Sluch, A. Godt, U. H. F. Bunz, M. A. Berg, *J. Am. Chem. Soc.* **2001**, *123*, 6447.
[19] A. Pogantsch, G. Heimel, E. Zojer, *J. Chem. Phys.* **2002**, *117*, 5921.
[20] H.-S. Im, E. R. Bernstein, *J. Chem. Phys.* **1988**, *88*, 7337.
[21] I. Cacelli, G. Prampolini, *J. Phys. Chem. A* **2003**, *107*, 8665.
[22] G. Heimel, M. Daghofer, J. Gierschner, E. J. W. List, A. C. Grimsdale, K. Müllen, D. Beljonne, J.-L. Brédas, E. Zojer, *J. Chem. Phys.* **2005**, *122*, 054 501.
[23] N. I. Nijegorodov, W. S. Downey, M. B. Danailov, *Spectrochim. Acta, Part A* **2000**, *56*, 783.
[24] The actual conjugation length is the number of conjugated π-bonds between two defects (in contrast to the ideal conjugation length, which is given as the number of monomers that constitute the oligomer times the number of π-bonds per monomer).
[25] U. Rauscher, H. Bässler, D. D. C. Bradley, M. Hennecke, *Phys. Rev. B: Condens. Matter Mater. Phys.* **1990**, *42*, 9830.
[26] E. Mulazzi, A. Ripamonti, J. Wery, B. Dulieu, S. Lefrant, *Phys. Rev. B: Condens. Matter Mater. Phys.* **1999**, *60*, 16 519.
[27] F. Negri, M. Z. Zgierski, *J. Chem. Phys.* **1994**, *100*, 2571.
[28] a) C. Manneback, *Physica* **1951**, *17*, 1001. b) W. Siebrand, *J. Chem. Phys.* **1967**, *46*, 440.
[29] U. Stalmach, H. Kolshorn, I. Brehm, H. Meier, *Liebigs Ann.* **1996**, 1449.
[30] J. Ma, S. Li, Y. Jiang, *Macromolecules* **2002**, *35*, 1109.
[31] D. Oelkrug, H.-J. Egelhaaf, D. R. Worrall, F. Wilkinson, *J. Fluoresc.* **1995**, *5*, 165.
[32] J. Bras, S. Guillerez, B. Peépin-Donat, *Chem. Mater.* **2000**, *12*, 2372.
[33] G. Bidan, A. De Nicola, V. Enée, S. Guillerez, *Chem. Mater.* **1998**, *10*, 1052.
[34] J.-S. K. Yu, W.-C. Chen, C.-H. Yu, *J. Phys. Chem. A* **2003**, *107*, 4268.
[35] O. Kwon, M. L. McKee, *J. Phys. Chem. A* **2000**, *104*, 7106.
[36] U. Salzner, P. G. Pickup, R. A. Poirier, J. B. Lagowski, *J. Phys. Chem. A* **1998**, *102*, 2572.
[37] U. Salzner, J. B. Lagowski, P. G. Pickup, R. A. Poirier, *Synth. Met.* **1998**, *96*, 177.
[38] D. Chakraborty, J. B. Lagowski, *J. Chem. Phys.* **2001**, *115*, 184.
[39] S. Suramitr, T. Kerdcharoen, T. Srikhirin, S. Hannongbua, *Synth. Met.* **2005**, *155*, 27.
[40] a) S. Yang, P. Olishevski, M. Kertsz, *Synth. Met.* **2004**, *141*, 171. b) M. Kertesz, C. H. Choi, S. Yang, *Chem. Rev,* **2005**, *105*, 3448
[41] a) D. A. dos Santos, D. Beljonne, J. Comil, J.-L. Brédas, *Chem. Phys.* **1998**, *227*, 1. b) D. Beljonne, Z. Shuai, R. H. Friend, J.-L. Brédas, *J. Chem. Phys.* **1995**, *102*, 2042. c) J. Cornil, D. Beljonne, C. M. Heller, I. Campbell, B. K. Laurich, D. L. Smith, D. D. C. Bradley, K. Müllen, J.-L. Brédas, *Chem. Phys. Lett.* **1997**, *278*, 139. d) J. Cornil, D. Beljonne, Z. Shuai, T. W. Hagler, I. Campbell, D. D. C. Bradley, J.-L. Brédas, C. W. Spangler, K. Müllen, *Chem. Phys. Lett.* **1995**, *247*, 425. e) J. Cornil, I. Gueli, A. Dkhissi, J. C. Sancho-Garcia, E. Hennebicq, J. P. Calbert, V. Lemaur, D. Beljonne, J.-L. Brédas, *J. Chem. Phys.* **2003**, *118*, 6615. f) D. Beljonne, J. Cornil, R. H. Friend, R. A. J. Janssen, J.-L. Brédas, *J. Am. Chem. Soc.* **1996**, *118*, 6453.
[42] A. Yang, M. Kuroda, Y. Shiraishi, T. Kobayashi, *J. Phys. Chem. B* **1998**, *102*, 3706.
[43] J. Seixas de Melo, L. M. Silva, L. G. Arnaut, R. S. Becker, *J. Chem. Phys.* **1999**, *111*, 5427.
[44] J.-F. Wang, J.-K. Feng, A.-M. Ren, X.-D. Liu, Y.-G. Ma, P. Lu, H.-X. Zhang, *Macromolecules* **2004**, *37*, 3451.
[45] H. Meier, U. Stalmach, H. Kolshorn, *Acta Polym.* **1997**, *48*, 379.
[46] a) N. Sumi, H. Nakanishi, S. Ueno, K. Takimiya, Y. Aso, T. Otsubo, *Bull. Chem. Soc. Jpn.* **2001**, *74*, 979. b) T. Otsubo, Y. Aso, K. Takimiya, H. Nakanishi, N. Sumi, *Synth. Met.* **2003**, *133–134*, 325.
[47] T. Izumi, S. Kobashi, K. Takimiya, Y. Aso, T. Otsubo, *J. Am. Chem. Soc.* **2003**, *125*, 5286.
[48] H.-J. Egelhaaf, L. Lüer, A. Tompert, P. Bäuerle, K. Müllen, D. Oelkrug, *Synth. Met.* **2000**, *115*, 63.
[49] H.-J. Egelhaaf, D. Oelkrug, W. Gebauer, M. Sokolowski, E. Umbach, T. Fischer, P. Bäuerle, *Opt. Mater.* **1998**, *9*, 59.
[50] a) H. Meier, *Angew. Chem. Int. Ed.* **2005**, *44*, 2482. b) H. Meier, J. Gerold, D. Jacob, *Tetrahedron Lett.* **2003**, *44*, 1915. c) H. Meier, J. Gerold, H. Kolshorn, W. Baumann, M. Bletz, *Angew. Chem. Int. Ed.* **2002**, *41*, 292. d) H. Meier, J. Gerold, H. Kolshorn, B. Mühling, *Chem. Eur. J.* **2004**, *10*, 360. e) H. Meier, B. Mühling, H. Kolshorn, *Eur. J. Org. Chem.* **2004**, 1033.
[51] G. Drefahl, R. Kühmstedt, H. Oswald, H.-H. Hörhold, *Makromol. Chem.* **1970**, *131*, 89.
[52] G. N. Patel, R. R. Chance, J. D. Witt, *J. Polym. Sci., Polym. Lett. Ed.* **1978**, *16*, 607.
[53] R. E. Martin, F. Diederich, *Angew. Chem. Int. Ed.* **1999**, *38*, 1350.
[54] J. Rissler, *Chem. Phys. Lett.* **2004**, *395*, 92.
[55] H. Becker, H. Spreitzer, W. Kreuder, E. Kluge, H. Schenk, I. Parker, Y. Cao, *Adv. Mater.* **2000**, *12*, 42.
[56] R. C. Johnson, in *Pade Approximations and their Applications* (Ed: P. R. Graves-Morris), Academic, London **1973**.
[57] K. Hirayama, *J. Am. Chem. Soc.* **1955**, *77*, 373. The empirical formula was justified by the author on the basis of the Lewis and Calvin model [58].
[58] G. N. Lewis, M. Calvin, *Chem. Rev.* **1939**, *25*, 273.
[59] A more general Lewis and Calvin model, accounting also for polymethin systems, was introduced in: S. Dähne, R. Radeglia, *Tetrahedron* **1971**, *27*, 3673.
[60] W. Kuhn, *Helv. Chim. Acta* **1948**, *31*, 1780.
[61] a) W. T. Simpson, *J. Am. Chem. Soc.* **1955**, *77*, 6164. b) A. Onipko, Y. Klymenko, L. Malysheva, *J. Chem. Phys.* **1997**, *107*, 7331. c) R. Chang, J. H. Hsu, W. S. Fann, K. K. Liang, C. H. Chang, M. Hayashi, J. Yu, S. H. Lin, S. E. C. Chang, K. R. Chuang, S. A. Chen, *Chem. Phys. Lett.* **2000**, *317*, 142. d) M. Bednarz, P. Reineker, E. Mena-Osteritz, P. Bäuerle, *J. Lumin.* **2004**, *110*, 225.
[62] W. J. D. Beenken, T. Pulleritis, *J. Phys. Chem. B* **2004**, *108*, 6164.

[63] a) H. Kuhn, *Fortschr. Chem. Org. Naturst.* **1958**, *16*, 169. b) H. Kuhn, *Fortschr. Chem. Org. Naturst.* **1959**, *17*, 404. c) G. Wenz, M. A. Müller, M. Schmidt, G. Wegner, *Macromolecules* **1984**, *17*, 837.
[64] a) M. J. S. Dewar, *J. Chem. Soc.* **1952**, *3532*, 3544. b) W. Kutzelnigg, *Theor. Chim. Acta* **1966**, *4*, 417. c) B. E. Kohler, *J. Chem. Phys.* **1990**, *93*, 5838. d) J. E. Lennard-Jones, *Proc. R. Soc. London Ser. A* **1937**, *158*, 280.
[65] a) S. Ramasesha, S. K. Pati, Z. Shuai, J.-L. Brédas, *Adv. Quantum Chem.* **2000**, *38*, 121. b) A. Race, W. Barford, R. J. Bursill, *Phys. Rev. B: Condens. Matter Mater. Phys.* **2003**, *67*, 245 202.
[66] For an early review see: L. G. S. Brooker, W. T. Simpson, *Annu. Rev. Phys. Chem.* **1951**, *2*, 121. More recently, Meier et al. reviewed different extrapolation approaches [45].
[67] M. C. Zerner, in *Reviews in Computational Chemistry*, Vol. 2 (Eds: K. W. Lipkowitz, D. B. Boyd), VCH, New York **1994**, p. 313.
[68] a) J. Cornil, D. A. dos Santos, X. Crispin, R. Silbey, J.-L. Brédas, *J. Am. Chem. Soc.* **1998**, *120*, 1289. b) J. Cornil, D. Beljonne, J.-L. Brédas, *J. Chem. Phys.* **1995**, *103*, 834.
[69] P. Tavan, K. Schulten, *J. Chem. Phys.* **1986**, *85*, 6602.
[70] S. Karabunarliev, M. Baumgarten, N. Tyutyulkov, K. Müllen, *J. Phys. Chem.* **1994**, *98*, 11 892.
[71] J. B. Lagowski, *J. Mol. Struct.* **2002**, *589–590*, 125.
[72] J. R. Reimers, Z.-L. Cai, A. Bilic, N. S. Hush, *Ann. N. Y. Acad. Sci.* **2003**, *1006*, 235.
[73] G. R. Hutchison, Y.-J. Zhao, B. Delley, A. J. Freeman, M. A. Ratner, T. J. Marks, *Phys. Rev. B: Condens. Matter Mater. Phys.* **2003**, *68*, 035 204.
[74] F. Schindler, J. Jacob, A. C. Grimsdale, U. Scherf, K. Muellen, J. Lupton, J. Feldmann, *Angew. Chem. Int. Ed.* **2005**, *44*, 1520.
[75] M. L. Renak, G. P. Bartholomew, S. Wang, P. J. Ricatto, R. J. Lachicotte, G. C. Bazan, *J. Am. Chem. Soc.* **1999**, *121*, 7787.
[76] Y. Sakamoto, S. Komatsu, T. Suzuki, *J. Am. Chem. Soc.* **2001**, *123*, 4643.
[77] M. Milián Medina, D. Beljonne, H.-J. Egelhaaf, J. Gierschner, unpublished.
[78] J. B. Lagowski, *J. Mol. Struct.* **2003**, *634*, 243.
[79] K. L. D'Amico, C. Manos, R. L. Christensen, *J. Am. Chem. Soc.* **1980**, *102*, 1777.
[80] L. Onsager, *J. Am. Chem. Soc.* **1936**, *58*, 1486.
[81] J. Gierschner, D. Oelkrug, in *Encyclopedia of Nanoscience and Nanotechnology*, Vol. 8 (Ed: H. S. Nalwa), American Scientific, Stevenson Ranch, CA **2004**, pp. 219–238.
[82] a) *Single Organic Nanoparticles* (Eds: H. Nakanishi, K. Sasaki), Springer, Berlin **2003**. b) D. Horn, J. Rieger, *Angew. Chem. Int. Ed.* **2001**, *40*, 4330.
[83] J. Tomasi, M. Persico, *Chem. Rev.* **1994**, *94*, 2027.
[84] B. Boldrini, E. Cavalli, A. Painelli, F. Terenziani, *J. Phys. Chem. A* **2002**, *106*, 6286.
[85] a) F. C. Spano, *J. Chem. Phys.* **2001**, *114*, 5376. b) R. M. Hochstrasser, M. Kasha, *Photochem. Photobiol.* **1964**, *3*, 317.
[86] D. Oelkrug, J. Gierschner, H.-J. Egelhaaf, L. Lüer, A. Tompert, K. Müllen, U. Stalmach, H. Meier, *Synth. Met.* **2001**, *121*, 1693.
[87] K. M. Gaab, C. J. Bardeen, *J. Phys. Chem. B* **2004**, *108*, 4619.
[88] E. Peeters, A. M. Ramos, S. C. J. Meskers, R. A. J. Janssen, *J. Chem. Phys.* **2000**, *112*, 9445.
[89] J. Gierschner, D. Oelkrug, H.-J. Egelhaaf, unpublished.
[90] J. J. Apperloo, L. Groenendaal, H. Verheyen, M. Jayakannan, R. A. J. Janssen, A. Dkhissi, D. Beljonne, R. Lazzaroni, J.-L. Brédas, *Chem. Eur. J.* **2002**, *8*, 2384.
[91] E. E. Havinga, C. M. J. Mutsaers, L. W. Jenneskens, *Chem. Mater.* **1996**, *8*, 769.
[92] M. Dietrich, J. Heinze, G. Heywang, F. Jonas, *J. Electroanal. Chem.* **1994**, *369*, 87.
[93] D. Oelkrug, A. Tompert, J. Gierschner, H.-J. Egelhaaf, M. Hanack, M. Hohloch, E. Steinhuber, *J. Phys. Chem. B* **1998**, *102*, 1902.
[94] H.-J. Egelhaaf, J. Gierschner, D. Oelkrug, *Synth. Met.* **2002**, *127*, 221.
[95] a) C. C. Wu, M. C. DeLong, Z. V. Vardeny, J. P. Ferraris, J. J. Gutierrez, *Synth. Met.* **2003**, *137*, 939. b) P. F. van Hutten, J. Wildeman, A. Meetsma, G. Hadziioannou, *J. Am. Chem. Soc.* **1999**, *121*, 5910.
[96] a) T. Siegrist, C. Kloc, R. A. Laudise, H. E. Katz, R. C. Haddon, *Adv. Mater.* **1998**, *10*, 379. b) L. Antolini, G. Horowitz, F. Kouki, F. Garnier, *Adv. Mater.* **1998**, *10*, 382.
[97] T. Granier, E. L. Thomas, D. R. Gagnon, F. E. Karasz, R. W. Lenz, *J. Polym. Sci., Part B* **1986**, *24*, 2793.
[98] R. D. McCullough, S. Tristram-Nagle, S. P. Williams, R. D. Lowe, M. Jayaraman, *J. Am. Chem. Soc.* **1993**, *115*, 4910.
[99] R. E. Gill, A. Meetsma, G. Hadziioannou, *Adv. Mater.* **1996**, *8*, 212.
[100] B. E. Kohler, *J. Chem. Phys.* **1990**, *93*, 5838
[101] S. Ramasesha, Z. G. Soos, *J. Chem. Phys.* **1984**, *80*, 3278.
[102] a) K. Schulten, M. Karplus, *Chem. Phys. Lett.* **1972**, *14*, 305. b) P. Tavan, K. Schulten, *J. Chem. Phys.* **1979**, *70*, 5407.
[103] a) R. Improta, F. Santoro, C. Dietl, E. Papastathopoulos, G. Gerber, *Chem. Phys. Lett.* **2004**, *387*, 509. b) A. Masunov, S. Tretiak, J. W. Hong, B. Liu, G. C. Bazan, *J. Chem. Phys.* **2005**, *122*, 224 505.
[104] B. Milián Medina, J. Gierschner, unpublished.
[105] a) A. P. Scott, L. Radom, *J. Phys. Chem.* **1996**, *100*, 16 502. b) J. M. L. Martin, J. El-Yazal, J. P. François, *J. Phys. Chem.* **1996**, *100*, 15 358
[106] H.-G. Mack, J. Gierschner, unpublished.
[107] J. C. Sancho Garcia, J.-L. Brédas, D. Beljonne, J. Cornil, R. Martinez Alvarez, M. Hanack, L. Poulsen, J. Gierschner, H.-G. Mack, H.-J. Egelhaaf, D. Oelkrug, *J. Phys. Chem. B* **2005**, *109*, 4872.
[108] Note that in the report by Pogantsch et al. the overestimation of the slope by TD-DFT, as observed for the other oligomer series, seems to be reversed for the ladder-type L*n*Ps [19]. However, the cited experimental value for L2P in this case is for fluorene, not the 2-ring oligomer homologue of the L*n*P series (which was not reported in literature) and should therefore not be used for comparison. By adding the experimental value for the 7-ring oligomer [16] instead (see Fig. 8), the usual overestimation of the slope by the TD-DFT method is obtained.
[109] F. C. Grozema, P. T. van Duijnen, L. D. A. Siebbeles, A. Goossens, S. W. de Leeuw, *J. Phys. Chem. B* **2004**, *108*, 16 139.
[110] S. Grimme, M. Parac, *ChemPhysChem* **2003**, *4*, 292.
[111] D. Delaere, M. T. Nguyen, L. G. Vanquickenborne, *Phys. Chem. Chem. Phys.* **2002**, *4*, 1522.
[112] G. Hutchison, M. A. Ratner, T. J. Marks, *J. Phys. Chem. A* **2002**, *106*, 10 596.
[113] S. M. Bouzzine, S. Bouzakraoui, M. Bouachrine, M. Hamidi, *J. Mol. Struct.* **2005**, *726*, 271.
[114] S. Bouzakraoui, S. M. Bouzzine, M. Bouachrine, M. Hamidi, *J. Mol. Struct.* **2005**, *725*, 39.
[115] Ampac, version 8.15; Semichem Inc., Shawnee KS **2004**.
[116] J. Cornil, D. Beljonne, J.-L. Brédas, *J. Chem. Phys.* **1995**, *103*, 842.
[117] S. Karabunarliev, M. Baumgarten, K. Müllen, *J. Phys. Chem. A* **2000**, *104*, 8236.
[118] U. Salzner, O. Karalti, S. Durdağı, *J. Mol. Model.* **2006**, *12*, 687.
[119] S. S. Zade, M. Bendikov, *Org. Lett.* **2006**, *8*, 5243.